IN-SITU S-PARAMETER ANALYSIS AND APPLICATIONS

A Thesis
Presented to
The Academic Faculty

by

Kyle Hershberger

In Partial Fulfillment
of the Requirements for the Degree
Master of Science in the
School of Electrical and Computer Engineering

Georgia Institute of Technology
May 2014

IN-SITU S-PARAMETER ANALYSIS AND APPLICATIONS

Approved by:

Professor James S. Kenney, Committee Chair
School of Electrical and Computer Engineering
Georgia Institute of Technology

Professor James S. Kenney, Advisor
School of Electrical and Computer Engineering
Georgia Institute of Technology

Professor John D. Cressler
School of Electrical and Computer Engineering
Georgia Institute of Technology

Professor Greg D. Durgin
School of Electrical and Computer Engineering
Georgia Institute of Technology

Date Approved: March 2014

ACKNOWLEDGEMENTS

To everyone who assisted during this overly long and drawn out ordeal.

Contents

List of Figures

SUMMARY

A methodology for obtaining RF network parameters of embedded RF networks is investigated and described. The frameworks discussed allow for one or two port S-Parameter matrices to be extracted from internal components of a RF network in-situ. The in-situ analysis allows these parameters to be extracted without having to alter any connections within the complete network. Detailed analysis of the aspects necessary to achieve correct results is performed and discussed. Three new methods for extracting different characteristics of a RF network are presented. In addition a brief overview of existing RF network stability analysis is covered. Finally a brief outline of the application of the various in-situ techniques for practical amplifier design.

Chapter I

INTRODUCTION

RF amplifier design is a process that contains numerous challenges, including achieving desired gain, output power, efficiency, size, and ensuring stability of the design. Techniques for approaching these design challenges in single stage amplifiers have been well discussed and have become elementary topics for RF circuit designers. These challenges become more difficult when multiple amplification stages are required to achieve the desired performance. The amount of published material available that covers the aspects of multi-stage RF amplifier design in depth is substantially less than for single stage designs. This thesis is concerned with the nature of the increased challenge of multi-stage amplifier design and with the development of analysis techniques to aid with overcoming these challenges.

A specific challenge with multi-stage RF amplifier design is understanding how the behavior of each of the stages changes as additional components are added to the design. Due to high levels of integration it is often difficult to isolate each of the amplification stages without appreciably compromising the performance of the design. As a result each stage will interact with the other stages around it, and this interaction must be understood and monitored. A weakness of the standard two-port network analysis techniques are that they only examine the input and output ports of a RF network. This results in the tendency to only analyze individual components/stage of the design before they are combined with each other. Once the circuity surrounding an amplification stage has been connected, it becomes difficult to reanalyze that stage without removing it again. This creates a situation where certain aspects of the amplifier design cannot be performed on the circuit as it actually will exist in the final design. This can result in undesired, and unexpected, behavior in the final design.

The analysis of RF amplifier stability is one such design task that suffers from the aforementioned problem. Most (if not all) of the stability analysis techniques commonly

known and used by design engineers are two-port analysis. This means that the only way to analyze the stability of an amplifier is to examine it all at once. One input port and one output port for the entire circuit. If an internal section of the amplifier is to be analyzed in more detail, it must be completely removed from the design so that access to the input and output ports of the sub-network can be achieved. When this is done, all the effects of circuitry surrounding that sub-network in the full design are lost. This is not a concern if the sub-network can be made to be unconditionally stable, but oftentimes the performance loss that results from unconditionally stabilizing a network precludes this approach.

This thesis will begin with an investigation on the limitations associated with the predominate two-port stability analysis techniques with respect to multi-stage RF amplifier design. The primary focus will be to investigate and develop network analysis techniques that allow internal ports to be created within a RF circuit. This technique will facilitate the application of existing stability analysis techniques in ways that are not commonly known. Examples of situations where traditional network and stability analysis is insufficient will be presented, and the application of the newly developed techniques will be examined.

Chapter II

EXISTING STABILITY ANALYSIS

The subject of active circuit stability has been a well established field of study, and as a result there are numerous stability analysis techniques that have been developed. Each of these techniques is tailored towards a particular design methodology. Some techniques are focused on loop analysis and yield themselves to the design methodology typically employed for analog / baseband circuits. Other loop analysis techniques are used in the context of RF network design and yield themselves towards oscillator analysis. Most of the techniques used in RF amplifier design are based upon two-port network analysis. Since two-port analysis is the most commonly used technique in RF amplifier design they will be the ones investigated in this section.

The stability analysis techniques in widespread use for RF amplifier design are based upon representing the circuit is as a two-port network. A benefit of this is that the entire operation of the circuit is simplified down to a single black box as shown in Figure 1. This is also a significant limitation as it does not provide an understanding of what is occurring within the circuit to generate the behavior of the two-port model. These techniques typically focus on the effect that a termination on one port of network will have upon the impedance seen looking into the the other, un-terminated, port. If it can be shown that the impedance seen looking into one of the ports of a two-port network remains passive for any and all possible passive terminations applied to the other port then the network is said to be unconditionally stable. In this case passivity is defined as the real part of the impedance (or admittance) being non-negative with no constraint on the imaginary component. Additional techniques investigate the situation that results in the event that the impedance of a two-port does not remain passive for all possible terminations.

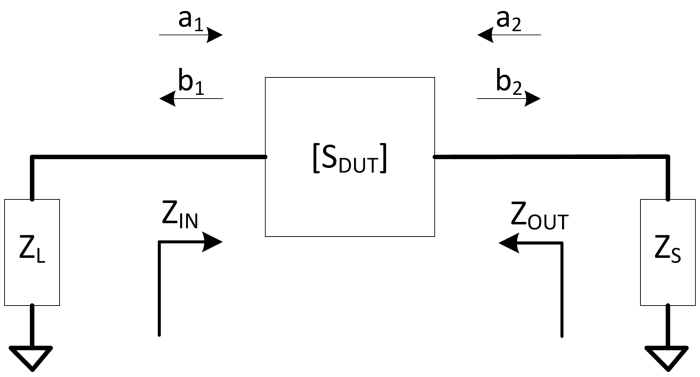

Figure 1: Block diagram of basic two-port analysis

2.1 Rollet's

Rollet's k-factor is arguably the best known out of all the common two-port stability analysis techniques. As such it will be the first one to be investigated. This technique was first introduced by Rollett in 1962 with his paper "Stability and power gain invariants of linear two-ports." [3] The premise of this analysis technique is to provide a method for determining if a two-port network is unconditionally stable. This is accomplished by creating a set of conditions that, if satisfied, will guarantee that the two-port is unconditionally stable. The results of Rollet's analysis can be stated in multiple different ways, but the most straightforward is shown in Equations 1 and 2.

For a two port network to be considered unconditionally stable the quantity, K, as defined in Equation 1 must be greater than unity at all frequencies. A supporting condition that must also be met is that the quantity defined in Equation 2 must be less than unity for all frequencies. Both of these conditions must be simultaneously met in order for the two-port network to be considered unconditionally stable.

$$K = \frac{1 - |S_{11}|^2 - |S_{22}|^2 + |\Delta|^2}{2\,|S_{12}.S_{21}|} > 1 \tag{1}$$

$$|\Delta| = |S_{11}.S_{22} - S_{12}.S_{21}| < 1 \tag{2}$$

There are numerous limitations to this approach that have been discussed in literature.

One such limitation is that this analysis suffers from being unable to predict unstable conditions if any poles exist in the right hand plane. [12] In situations where such poles exist, the criteria provided above can provide a false indication that a two-port is unconditionally stable when in fact potential instabilities exist within the network. Additional notable limitation is that when the above criteria are not met there is little insight to be gained as to the actual level of instability present. [6] Often times designers will make the incorrect assumption that larger values of K are a certain indication of increased stability of the two-port.

2.2 Mu

Another common two-port stability analysis technique is the use of the Mu criterion. The Mu criterion was developed as a more thorough and robust replacement for Rollet's K factor. The original derivation of this criterion is presented in [6] and the expressions for the criteria are shown in Equations 3 and 4. The details of the derivation will be spared for this discussion as they are well described in [6]. The Mu criterion is based on a graphical mapping technique to determine the minimum distance between the origin of the Smith chart and the nearest region of instability. In other words, Mu represents the minimum magnitude of reflection that has to be applied to either port of the two-port in order for a potential unstable operating condition to exist. Thus by ensuring that Mu is always greater than unity one can ensure that a two-port network is unconditionally stable for all passive terminations. Equations 3 and 4 are duals of each other and either expression is a necessary and sufficient condition for unconditional stability. It is not necessary to compute both quantities.

$$\mu = \frac{1 - |S_{11}|^2}{|S_{22} - \Delta \cdot S_{11}^*| + |S_{12}.S_{21}|} > 1 \tag{3}$$

$$\mu\prime = \frac{1 - |S_{22}|^2}{|S_{11} - \Delta \cdot S_{22}^*| + |S_{12}.S_{21}|} > 1 \tag{4}$$

$$\Delta = S_{11} \cdot S_{22} - S_{12} \cdot S_{21}$$

The Mu stability criterion solves the two major drawbacks of K factor analysis. The expression handles all special cases that can potentially lead the K-factor analysis to falsely indicate unconditional stability. In addition it provides a single numeric value that captures the stability condition of the network that has a graphical significance and interpretation. Since Mu represents the minimum distance from the origin to an unstable region it directly corresponds to the maximum reflection coefficient that may be applied before a network is no longer stable. So even if Mu is less than unity it will still provide a designer with a measure of how close the network is to being unstable.

2.3 Limitations of existing techniques

There are several limitations to the existing analysis techniques discussed in this section. Most notably are that they only investigate the external behavior of a network since they are limited to only interacting with the two external ports. The traditional workaround to the limitations of these techniques has been to divide a design into discrete sections and perform the above analysis on each section individually. The idea being that if each section can be shown to be unconditionally stable, or at least at an acceptable level of conditional stability that the combination of these components will be stable. In the case of ensuring that each discrete segment of the design offers unconditional stability a major drawback is that performance is typically degraded resulting from the detuning or addition of loss necessary to stabilize the network. In the cases where conditional stability of the discrete segments is allowed, in depth loading analysis must be performed to ensure that the loading that adjacent segments provide to each other stay within the conditionally stable region.

There are several problems with either of these approaches. Most notably that they are tedious and prone to error. In order for each discrete analysis to be indicative of the combined performance, the loading condition caused by the surrounding blocks must be considered when performing the analysis. While this is not a insurmountable task it does require care during the analysis process. Care must also be taken to ensure that crucial interactions between circuit elements are maintained and not disturbed when the circuit is divided. An example of circuit interactions could be a feedback loop caused by supply

network interaction. In this hypothetical case signal is injected into the supply network by one of the final stages of a multi-stage amplifier that is then picked up by the supply connection in a preceding stage. If the design was then divided stage-by-stage this interaction would inherently be broken. Thus the premise that the individual stability analysis being performed would be be representative of the cascaded system is flawed.

Chapter III

TECHNIQUES FOR IN-SITU ANALYSIS

This section will focus on the investigation of various techniques for obtaining network parameters in-situ. In this context the term in-situ refers to a measurement technique that does not disturb the natural operation of the circuit. Thus the behavior of the network remains unchanged whether the analysis is being performed or not. The end goal is to be able to investigate the behavior of the network exactly as it is during normal operation.

For this application the desire is to create a device, or probe, that can be placed in series with a transmission path in the network to be analyzed. The transmission path to be analyzed is identified and a splice is created as shown in Figure 2. The probe will then be inserted between the two ends of the splice as shown in Figure 3. By placing the probe in series it will be able to sense the operational condition of the network looking in both directions away from the splice. In order for the probe to be truly in-situ, the presence of the probe in the circuit cannot change or perturb the operation of the circuit in any way. This is achieved by making the transmission path through the probe as close to an ideal zero length through (short circuit) as possible. This implies zero series impedance and infinite shunt admittance in terms of circuit parasitics, and zero insertion loss and zero insertion phase in terms of network characteristics. The two ports of the probe that are used to connect to the circuit form a two-port network characterized by the S-matrix of Equation 5. The end result is a component in the circuit that does not alter the transmission or reflection characteristics of the network components it was inserted between, but is still able to obtain the necessary information to provide the desired results.

$$S_{INSITU} = S_{THRU} = \begin{bmatrix} 0 & 1 \\ 1 & 0 \end{bmatrix} \tag{5}$$

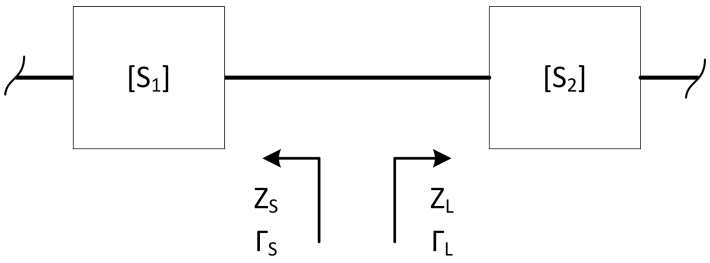

Figure 2: Block diagram illustrating interface between two-port networks.

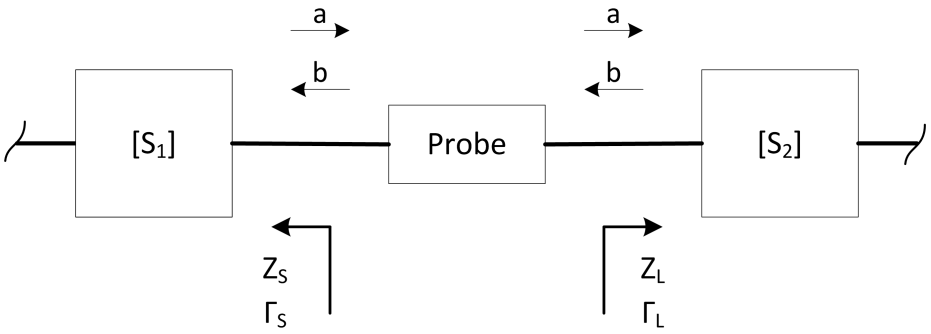

Figure 3: Block diagram showing S-Probe inserted between two networks.

3.1 Requirements for accurate in-situ analysis

Before the various methods for creating in-situ probes are investigated it is crucial that a in depth investigation is done on the environment into which these probes will be placed. Because this environment is typically a real-world multi-stage active network many of the simplifying assumptions that are used during traditional two-port analysis are no longer valid. If this is not taken into consideration incorrect results are obtained. A large portion of the research that went into these techniques was focused on how to handle the more complex environment presented by these complex networks. In addition some simpler techniques may appear to provide valid results in a more benign environment, but they break down when placed into a more complicated environment. Rather than spend time presenting these simpler, yet flawed, methods the derivations will focus on accounting for complex environments from the beginning. This will yield a result that may seem overly complicated, but the additional complexity is necessary for handling the situations that arise in complex networks.

The primary benefit of the in-situ probe, which is the fact that it exists in series with a

transmission path in a network, is also the primary source of complications. When the basic functions of an in-situ probe are considered it is easy to imagine that it is simply dividing the network at the location of the probe. This is not actually the case since dividing the network would violate one of the central tenants of in-situ analysis. The probe must be able to analyze the behavior looking into the ports connected on each side of the probe while not disrupting the interaction of the two ports under observation. The resulting complications that arise from the ports under analysis remaining coupled can be separated into two classifications. These classifications being those of a mismatched terminations and those caused by feedback. Both causes ultimately result in the same phenomena of multiple incident waves being applied to the ports under analysis. In the case of mismatched terminations it is a result of the initial reflection from the port under analysis being re-reflected by the opposing port. The challenge is to account for the effect of this additional incident wave. In the case of feedback additional waves can incident upon the port under analysis that occur as a result of feedback paths coupling the initial excitation in such a way that an additional incident wave emerges from the opposing analysis port.

An example of a circuit that contains both of these mechanisms is shown in Figure 4. This network is comprised of a two-port block (S_{DUT}) intended to represent an active circuit, but the nature of this two-port isn't critical. This block is then surrounded on both sides by two additional two-port networks (S_{IN} and S_{OUT}) with non-zero reflection coefficients for the ports facing to the original two-port (S_{DUT}). Finally a feedback network (S_{FB}) is coupling the output of the overall network back into it's input. There are two copies of the circuit in the figure. The top network is intended to be the model used to generate the correct result. The method of analysis to obtain the true result to use as a reference is to run an AC simulation and inject a test current into the node labeled V_{TEST} at port 1 of S_{DUT}. The total impedance seen looking into this node is then V_{TEST}/I_{TEST} . The bottom network is intended to show what happens if the network is separated at the connection between port 2 of S_{IN} and port 1 of S_{DUT} . S-Parameter ports have been placed on both sides of the splice. S-Parameter port 3 looks back into the input network and will be used to determine the source impedance of the driving network and S-Parameter port 4 looks into the input

of S_{DUT} and will be used to determine input impedance of the loading network. The values of $Z_3$and Z_4will be calculated from the reflection coefficient returned by S-Parameter ports 3 and 4. The parallel combination of $Z_3$and Z_4 will then be used to determine the total impedance at that node. Since there is no frequency dependance defined for any of the elements in the network, the simulation will be performed at a single frequency point. The amount of feedback induced in the network will be swept over a range of values to show the effect that this has on the result.

Figure 5 shows the resulting node impedance calculated from both methods described above. In this graph $Z_{NODE} = Z_3 \cdot Z_4/(Z_3 + Z_4)$ is represented by the red circles and $Z_{TEST} = V_{TEST}/I_{TEST}$ is represented by the blue crosses. It can be seen that as the magnitude of the feedback M_{FB} approaches zero the two impedances converge on the same result. This intuitively makes sense since without feedback there is no coupling between the two halves of the circuit and the impedance calculation is trivial. As the magnitude of feedback increases the results diverge. In fact the result predicted by the S-Parameter ports does not vary at all while the result predicted by the test current method varies dramatically. This result shows the importance of ensuring that the operation of the circuit is not disrupted by the probe. It also shows that if feedback is present that it will have a significant impact on the behavior of the circuit.

The location from which the excitation signal is injected into the circuit must also be known and controlled in order to obtain correct results. The implications of this requirement depend on the type of probe being implemented, but all methods will yield incorrect results if unless this is well controlled. The effects of a high-reflection conditions and feedback loops will often invalidate assumptions as to the effective source of excitation unless steps are taken to explicitly guarantee it's source. This is the reason that all of the probes discussed in this section have internal sources. By providing their own excitation they are able to ensure that the nature of the excitation signal is precisely known. Examples of these conditions and the appropriate solutions will be examined as they become relevant in the following sections.

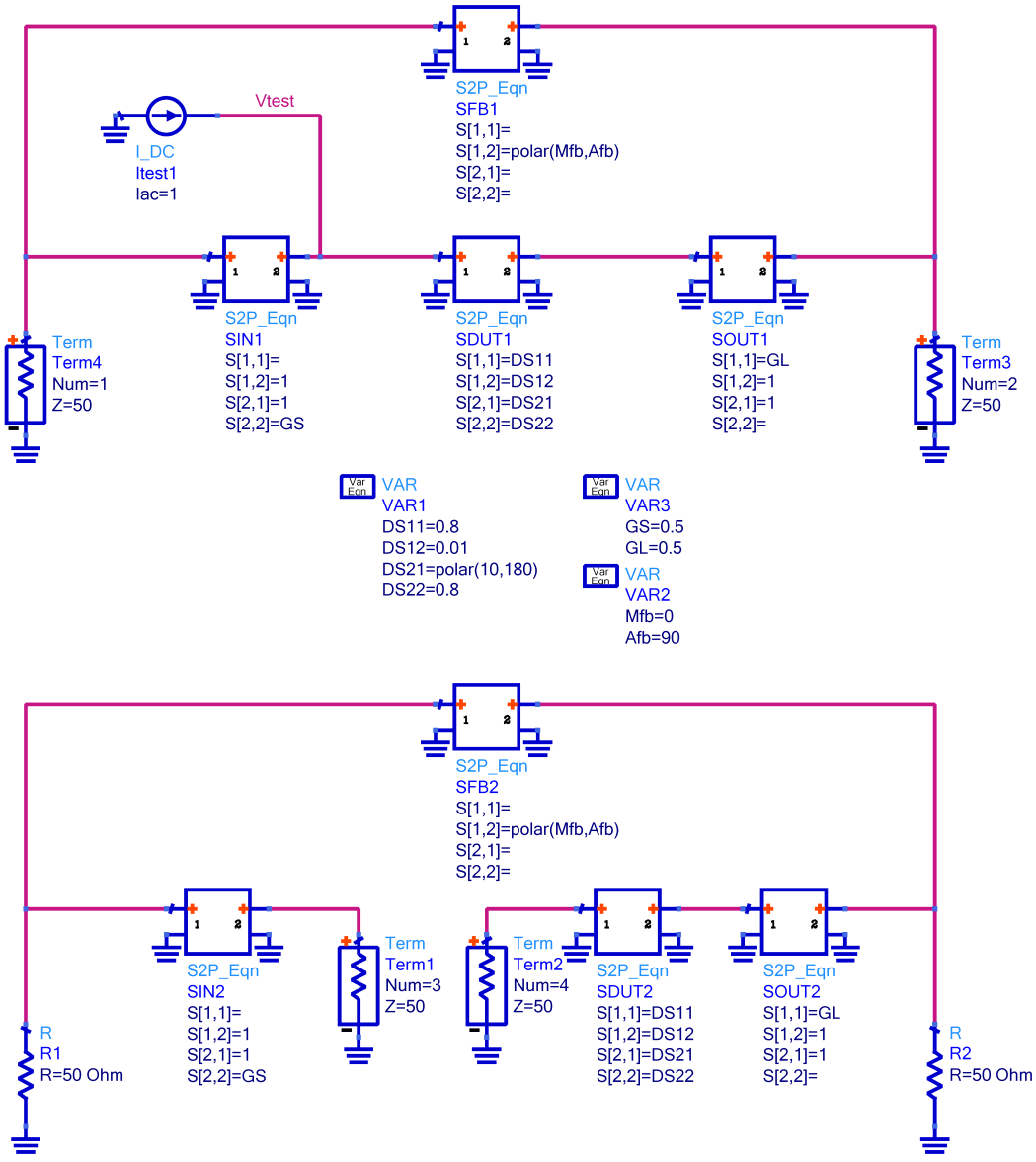

Figure 4: ADS Schematic of simplified circuit containing feedback and mismatched terminations

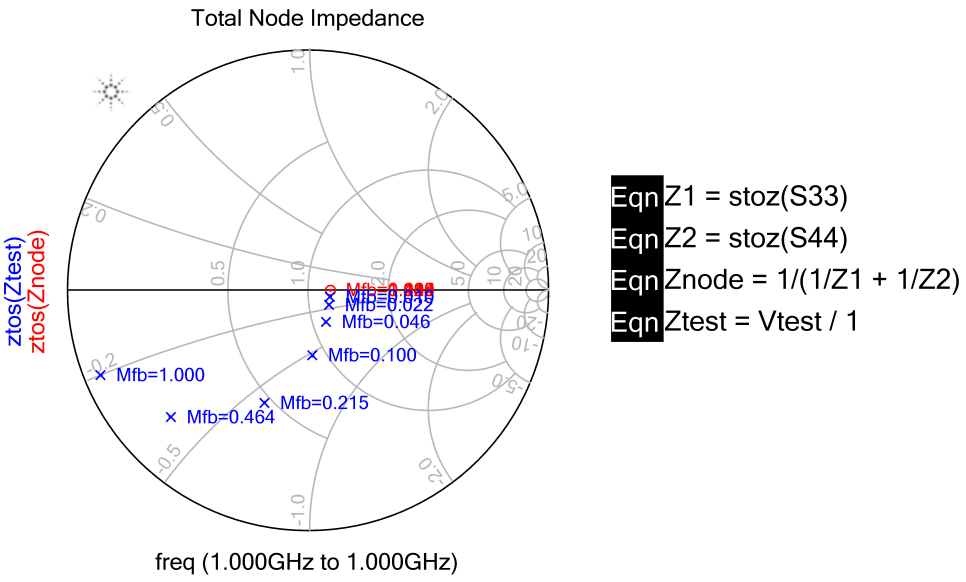

Figure 5: Smith Chart plotting calculated impedances as a function of feedback.

3.2 In-situ techniques

There are several approaches to creating accurate in-situ probes that can be used in S-Parameter simulation.This section will cover four different methodologies and discuss their derivation and associated strengths and weaknesses. There are additional techniques that will not be covered as they do not maintain accuracy for all potential environments into which they may be placed. In general these other approaches are special cases of the techniques presented here. Particular situations that cause problems for each of the techniques will be discussed when applicable. In general, the resulting network parameters generated by each of the techniques is similar. Although some techniques are capable of generating results not achievable by others.

3.2.1 S-Probe - VCVS

The first technique is developed around the concept of directly measuring the voltages and currents at each of the probes two analysis ports. This is achieved by injecting a test current from each of the probe ports into the attached network and then measuring the resulting voltage. The ratio of the resulting voltage to incident current is taken and Ohm's law is used to arrive at the effective impedance. It is important to note that all quantities involved in

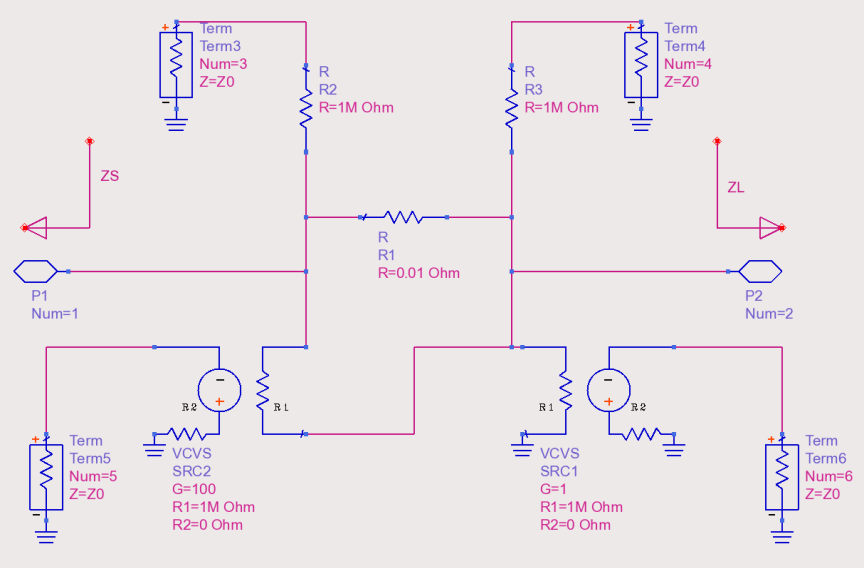

Figure 6: Schematic of Agilent ADS implementation of voltage-current based S-Probe

this analysis are complex phasors. The original methodology was shown in [1] and further refinements and implementations have been introduced. This technique has been in existence for several decades yet it does not seem to find widespread use amongst amplifier designers.

Figure 6 shows the circuit implementation of this probe as provided in the Agilent ADS simulation environment. This implementation has several enhancements beyond the original embodiment presented in [1]. Unfortunately there are no documented references provided in the Agilent documentation, so it is difficult to determine the history behind the additions to this probe implementation. This history would be enlightening as these enhancements dramatically improve the robustness of this probe. At present the only known documentation to the author on this implementation is that provided in [5]. For this type of in-situ probe the Agilent implementation will be the only embodiment considered. This is because the original implementation provided in [1] breaks down when placed into complex circuit environments such as shown in Figure 4.

It is useful to examine an example circuit to understand the rationale for the additional components present in the circuit of Figure 6 as compared with the implementation originally presented by [1]. Figure 7 shows a highly simplified circuit that can be used to exemplify the potential problems for this type of in-situ probe that are resolved by these additions.

In order to determine the impedance of a circuit branch either all independent sources in that branch must be zeroed or the value of the independent sources in that branch must all be known. This is illustrated by taking the circuit of Figure 7 and assuming that V_A and V_B are both open circuits, and that the voltage gain of the controlled source is $A_V = 0$. This reduced circuit is described by the system of Equations 6 and 7. In this system there are two equations and three unknowns, and as a result the system cannot be solved. However, Equation 7, which represents the passive, non-driven, branch has only one unknown. Since the quantity $(v_1 - v_2)/R_C$ is the current through the current sensing resistor R_C and is thus known. This allows for the impedance of the leg without the independent source to be directly solved for with the available information. The equation representing the leg with the independent source still cannot be solved without knowing the value of the independent source. The end result of this is that any independent sources with unknown values must not be contained within any circuit leg whose impedance is unknown. This is the reason for the additional excitation ports in the in-situ probe. By using explicit sources it ensures that the excitation source is always external to the circuit being measured. The reason for having two sources in the probe is that it makes calculating the impedances easier. If the current sensing resistor is always in between the excitation source and the circuit leg of interest, the impedance can be directly solved for. Assuming v_1 and v_2 are essentially identical by virtue of R_C being small compared to the surrounding impedances the resultant impedance is $Z_2 = v_1/I_C$ when V_A is the excitation source and $Z_1 = -v_1/I_C$ when v_B is the excitation source.

$$\frac{v_1 - v_S}{Z_1} + \frac{v_1 - v_2}{R_C} = 0 \tag{6}$$

$$-\left(\frac{v_1 - v_2}{R_C}\right) + \frac{v_2}{Z_2} = 0 \tag{7}$$

The circuit in Figure 7 can also be used to investigate the effect of feedback on the effective impedances of the circuit. In this case the independent source $V_S$will be zeroed to remove it's effect from the circuit. In this case V_A and V_B are again assumed to be open-circuits. The behavior of this version of the circuit is described by Equations 8 and 9. These

two equations setup a system with two unknowns since the quantity $(v_1 - v_2)/R_C$ is once again the current through resistor R_C and is thus known. The resulting expression for Z_1 is shown in Equation 10. There are two terms in this equation. The first term is equal to the direct resistance of the branch if no feedback was present and is thus independent of A_V. The second term is the effect of the feedback in the circuit and is a function of A_V. This equation shows that the apparent impedance of the left hand circuit branch will vary as the feedback term A_V is varied. If the left and right hand sides of the circuit are separated by removing R_C then the feedback term will also disappear as a result of v_2 being zero. RemovingR_C is analogous to the split in the bottom circuit of Figure 4. This illustrates that in order to obtain the correct impedance of a circuit branch all branches connected to a node must be excited during the analysis.

$$\frac{v_1 - A_V \cdot v_2}{Z_1} + \frac{v_1 - v_2}{R_C} = 0 \tag{8}$$

$$-\left(\frac{v_1 - v_2}{R_C}\right) + \frac{v_2}{Z_2} = 0 \tag{9}$$

$$i_1 = -\left(\frac{v_1 - v_2}{R_C}\right)$$

$$Z_1 = \frac{v_1}{i_1} - \frac{A_V \cdot v_2}{i_1} \tag{10}$$

The probe shown in Figure 6 is implemented using controlled sources, a current sensing resistor, and four S-Parameter ports. The probe is connected to the network to be analyzed using pins P1 and P2. The probe can be divided into two sections. The first section is comprised the sensing elements that are used to measure the current and voltages. The second section are the sources that are used to induce the test current.

The sensing components are comprised of the current shunt R1, voltage controlled voltage sources SRC1 and SRC2, and the two S-Parameter analysis ports 5 and 6. Controlled source SRC1 measures the voltage potential between the transmission path and ground and applies the same potential difference to analysis port 6. Thus causing the signal at port 6 to be

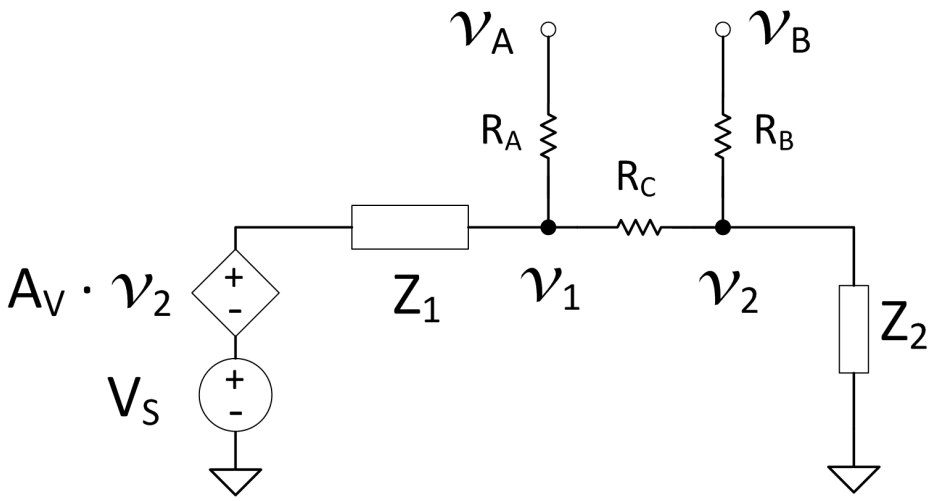

Figure 7: Example circuit to illustrate effect of independent sources and feedback on impedance calculation.

directly proportional to the voltage at the analysis nodes. Controlled source SRC2 senses the voltage potential across current sensing resistor R1 and applies it to analysis port 5. By Ohms law the voltage generated across R1 is directly proportional to the current flowing through it. R1 is chosen to be sufficiently small as to be negligible when placed in series with the circuit being probed. The voltage gain of SRC2 is chosen such that the voltage applied to analysis port 5 is scaled at 1V per 1A of current through R1. This is simply the inverse of R1, as shown in Equation 11. Note that it does not really matter which side of the sensing resistor R1 that SRC1 senses from since R1 is small as compared to the surrounding impedances and the voltage difference is negligible.

$$A_{V,SRC2} = \frac{1}{R_1} \tag{11}$$

The sourcing components consist of analysis ports 3 and 4. Each of these ports is connected to either side of resistor R1 through resistors chosen to be much larger than any of the impedances in the circuit being probed. The resistors effectively turn the ports into current sources. Where port 3 is injecting current into the network on the same side of R1 as pin P2, and port 4 is injecting current into the network on the same side of R1 as pin P2. The location of these ports is important as discussed earlier in order to obtain a correct

result. Since the desire is to be able to measure the impedance connected to both pin P1 and pin P2 two sources are required.

Now that the construction of the probe has been established, the means for calculating the desired numeric quantities can be discussed. Assuming that the four S-Parameter ports utilize the same numbers in simulation as shown in Figure 6, the simulator will return the needed information within the resultant S-matrix. Equation 12 shows how the impedance of the network connected to pin P1, referred to as Z_1, can be obtained from the resultant S matrix. The final results for obtaining both Z_1 and Z_2 is shown in Equations 13 and 14 respectively.

$$Z_1 = \frac{V_1}{I_1} = \frac{V_6}{\frac{V_5}{A_{V,SRC3} \cdot R_1}} = \frac{V_6}{V_5} = \frac{\frac{V_6}{V_4}}{\frac{V_5}{V_4}} = \frac{S_{64}}{S_{54}} \tag{12}$$

$$Z_1 = \frac{S_{64}}{S_{54}} \tag{13}$$

$$Z_2 = \frac{S_{63}}{S_{53}} \tag{14}$$

This analysis technique benefits from being inherently robust to problems caused by feedback and reflections. This is a result of the technique directly measuring the quantities of interest and all loading effects are inherently accounted for. The primary limitations of this technique are that it can only return the closed loop loaded impedances of the network connected to the probe's analysis pins and that four additional S-Parameter ports are required to provide the necessary excitation and sensing elements. The limitation of only providing closed loop results is primarily an issue when the circuit under analysis is exhibiting undesirable behavior. The additional S-parameter ports are an on-going burden. While they are of little concern for smaller analysis, the additional ports can result in very large S-Matrices when numerous probes are placed in a large circuit.

3.2.2 S Probe - Coupler

Another technique for creating an in-situ probe is by observing the forward and reverse waves passing through the probe and then using them to calculate reflection coefficients.

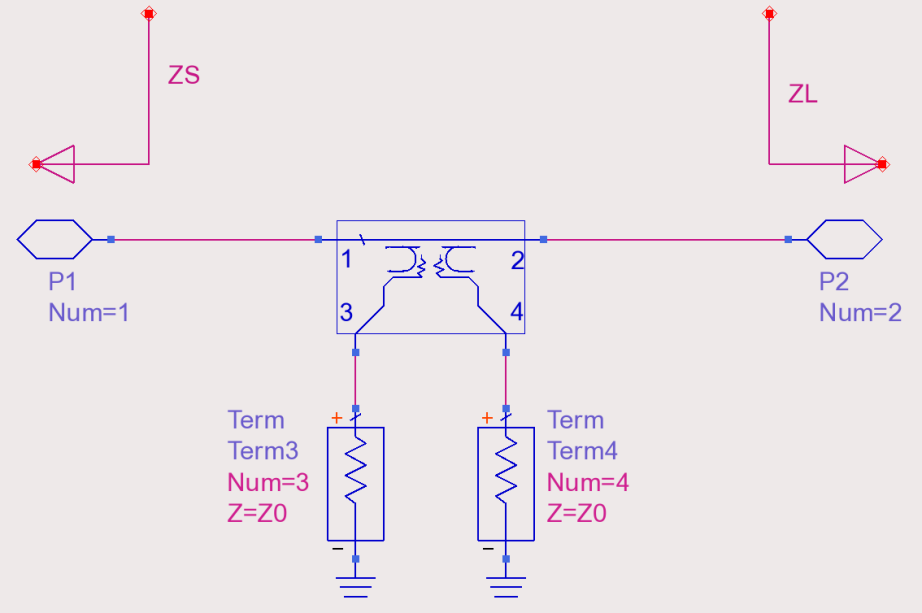

Figure 8: Schematic showing implementation of coupler based S-Probe

This is accomplished through the use of a directional coupler as shown in Figure 8. Since this technique uses quantities native to the S-Parameter simulation there are no additional circuit components required beyond a directional coupler and two S-Parameter ports.

As with the previous probe, this implementation also contains two functional components - a sourcing component and a sensing component. In this case the sourcing and sensing can be performed by the same circuit elements. For sensing, the directional coupler is used to provide a scaled copy of the forward wave to analysis port 3 and a scaled copy of the reverse wave to analysis port 4. For the purposes of this discussion the forward wave will be defined as the wave entering into the IN terminal of the probe and exiting the OUT terminal. The reverse wave will be the wave entering through the OUT terminal and exiting the IN terminal. Analysis ports 3 and 4 also function as the excitation sources in the analysis. Excitations generated by these ports are coupled into the network by virtue of the directional coupler. Energy from analysis port 3 is directed out of the probe's IN terminal in the reverse direction, and energy from port 4 is directed out of the probe's OUT terminal in the forward direction. These ports are used to create the incident waves required to excite the network.

The basic premise of the operation of this probe is to generate an incident wave using the

auxiliary S-Parameter ports and direct it into the network and then measure the resulting forward and reverse waves using the same auxiliary ports.. The ratio of the reflected wave to the forward wave is then calculated to obtain the reflection coefficient as described by Equation 15. In this equation b refers to the reflected wave that is being reflected by the port under analysis and a refers to the forward wave that is incident upon the port under analysis. The challenge is how to generate an incident wave that properly excites the circuit and while also obtaining correct values for both the a and b waves.

$$\Gamma = \frac{b}{a} \tag{15}$$

A crucial component of this probe is the directional coupler and as such is worthwhile to discuss the specifics of its implementation. Any coupler can fill the functional role required by this probe as long as it meets three key requirements. The first is that the coupler provide as close to an ideal through between the two in-situ analysis ports as possible. The second requirement is that it couples forward waves in the transmission path to one of the coupled ports and reverse waves in the transmission path to the other coupled port. The third requirement is that waves incident upon either of the coupled ports are coupled into forward or reverse waves in the transmission path with the direction dependent on which coupled port the signal is incident upon. If these requirements are met then the coupler can achieve the necessary functionality. A discussion of various couplers and details on the implementation of the one used in the following analysis is provided in Appendix A.2.

An appropriate place to start the investigation of an appropriate coupler design for this application is to examine the behavior of a idealized passive coupler. An example S matrix for a typical coupler is shown in 16. For this example the port designations are assigned according to the symbol in Figure 8. In this example C refers to the coupling factor of the coupler which will be a non-zero value less than unity. Upon examination of the S matrix it can be seen that the requirement of providing a relatively ideal short circuit is provided by S_{11} and S_{22} being zero and the transmission terms S_{12} and S_{21} approaching unity for values of C sufficiently small. Additionally it can be observed that the only signal appearing on port 3 will be a copy of the incident signal on port 1 scaled by the coupling factor and

that any signal incident upon port 3 will only be directed to port 1and also scaled by the coupling factor. This is captured by S_{13} and S_{31} being set equal to C. Port 4 has the same relationship with port 2 as port 3 does with port 1 as can be seen by S_{24} and S_{42} being set equal to C . All other terms are zero creating complete isolation between the various functions of the coupler. Thus all of the requirements of the coupler for use in an in-situ probe are satisfied. As the value of the coupling factor C decreases the ideal nature of the through condition improves.

$$S_{coupler} = \begin{bmatrix} 0 & \sqrt{1-C^2} & C & 0 \\ \sqrt{1-C^2} & 0 & 0 & C \\ C & 0 & 0 & 0 \\ 0 & C & 0 & 0 \end{bmatrix} = \begin{bmatrix} S_{11} & S_{12} & S_{13} & S_{14} \\ S_{21} & S_{22} & S_{23} & S_{24} \\ S_{31} & S_{32} & S_{33} & S_{34} \\ S_{41} & S_{42} & S_{43} & S_{44} \end{bmatrix} \tag{16}$$

A downside with the coupler model shown in 16 is the non-ideal through characteristic and the scaling / coupling factor existing in both directions. Since the coupled signals are being scaled for both the excitation wave and the measured waves additional terms in the equations developed in the following sections would be required. Since the entirety of this analysis is being performed n the simulation realm there is no requirement that the coupler model obey the restrictions imposed upon physically realizable couplers. Most notably is the requirement of passivity. If passivity is ignored a more suitable coupler model for in-situ probes is shown in 17. In this case the S_{12} and S_{21} terms are set to unity, thus creating an ideal through between ports 1 and 2. In addition different values for the coupling factors can be used depending on whether the coupling is being used for excitation or for sensing. To do this the S_{31} and S_{42} terms which represent the coupling used from transmission path waves into the sensing ports can be set to C_S. In addition the S_{13} and S_{24} terms which represent the coupling from the excitation ports into the transmission path are set to C_E. For ease of analysis and derivation of formulas it is convenient to set C_S to be unity. This results in the coupled signals of the forward and reverse waves appearing at ports 3 and 4 being verbatim copies of the forward and reverse waves respectively. This removes the need to carry around a scaling factor in the resulting analysis In addition the C_E term may be chosen to be any value greater than zero. A convenient value would again be unity, but for

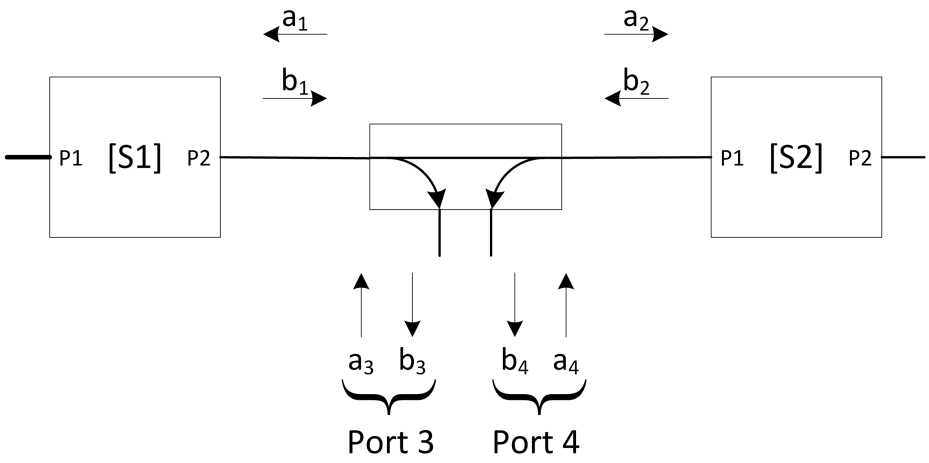

Figure 9: Block diagram of coupler based S-Probe inserted between two networks.

legacy reasons the C_E term has been left as a constant in the analysis. It is valid to set C_E to unity in this S matrix and all the following equations. The coupler model shown in Matrix 17 with C_S set to unity will be the one used for all further analysis using this type of in-situ probe.

$$S_{coupler} = \begin{bmatrix} 0 & 1 & C_E & 0 \\ 1 & 0 & 0 & C_E \\ C_S & 0 & 0 & 0 \\ 0 & C_S & 0 & 0 \end{bmatrix} \tag{17}$$

In order for this probe to provide a robust solution in complex circuits such as in Figure 4 care must be taken when determining how to excite the circuit and how to formulate the resulting reflection coefficient calculations. The requirements for a proper circuit excitation are the same as those illustrated in Figures 4 and 7. In the previous cases it was necessary to ensure that the test currents had access to both sides of the in-situ interface. In this case it is necessary to ensure that a incident wave is directed to both sides of the in-situ interface simultaneously. This is accomplished by creating a common-mode excitation on the coupled ports of the coupler which will result in the common-mode wave being equally split and directed into each of the in-situ ports by virtue of the directional coupler.

To begin deriving the formulas for calculating the source and load reflection coefficients

the wave quantities to be used in the analysis need to be defined and quantified. Figure 9 shows a block diagram with these quantities labeled. The designation of Port 1 is assigned to the source interface of the in-situ probe and Port 2 is assigned to the load interface of the probe. Port 3 is connected to the forward coupled port and Port 4 is connected to the reverse coupled port. The naming of the wave quantities follows the convention of the a wave being the incident wave and the b wave being the reflected wave.

The first step towards obtaining the reflection coefficients is to identify all the contributing components of the total forward and reverse waves. For now only the reflection condition on Port 1 will be considered. It will later be shown that the resulting equation for the reflection condition on Port 2 is a dual of that for Port 1. Equations 18 and 19 show the forward and reverse waves defined in terms of the waves sourced and sensed by ports 3 and 4. The b_1 term is the most straightforward to understand. Due to the operation of the coupler the b_3 wave will be be an exact copy of the b_1 wave due to $C_S = 1$ for the coupler being used in this derivation. Since there are two excitation sources there will be two separate contributing terms to b_1, one from each of the excitation sources. Superposition can used to sum these two contributors into a single quantity for b_1 because this analysis is being performed on a linear system. This is denoted by setting one of the sources to zero for each term.

The a_1 term is more complicated. There are three individual terms that comprise the a_1 wave. The primary contributor is the a_3 incident wave created by the port 3 source. Since this wave is coming from the coupled port it is scaled by the coupling factor $C_E = C$. The second and third terms are present to account for any energy that may be emerging from port 2 as a result of the a_3 and a_4 excitations respectively. It should be noted that these terms are present to ensure the probe maintains accurate results in high-reflection and feedback environments. In a well matched environment both the second and third terms will be near-zero. In complex environments such as in Figure 4 these terms are crucial in order to account for stray reflections caused by the excitation waves. Again superposition is used to combine the contributions from each excitation wave into a single quantity.

The next step is to divide each of these resulting wave quantities by the common mode excitation source as shown in Equations 20 and 21. This step converts each of the terms in

Equations 18 and 19 into a mixed-mode reflection coefficient. This represents the simultaneous excitation of both port 3 and 4 which is critical for obtaining the correct response. Since each of the terms has already been separated into the individual contributions from ports 3 and 4 the denominators may be simplified by appropriately setting either the a_3 or a_4 term to zero. This is shown in Equations 22 and 23. Once this simplification is performed it is clear that each of the terms on the right hand side may now be re-written as an S-parameter term from the simulation S-matrix. The left hand side still represents a mixed-mode reflection coefficient, but this is in fact the desired reflection coefficient for the input in-situ port, since it represents the total reflected energy as a function of the total energy incident upon the node. The final reflection coefficient is obtained by computing by dividing Equation 23 by Equation 22. It is important to remember that Equations 22 and 23 were derived assuming that a_1 is the incident wave and b_1 is the reflected wave. Thus the only reflection coefficient that be obtained from these equations is that of Γ_1 which is shown in Equation 24. The same process can be followed using a_2 as the incident wave and b_2 as the reflected wave to obtain Γ_2 as shown in Equation .25.

$$a_1 = [C \cdot a_3 + b_4]_{a_4=0} + [b_4]_{a_3=0} \tag{18}$$

$$b_1 = [b_3]_{a_4=0} + [b_3]_{a_3=0} \tag{19}$$

$$\frac{a_1}{a_3+a_4} = \left[\frac{C\cdot a_3+b_4}{a_3+a_4}\right]_{a_4=0} + \left[\frac{b_4}{a_3+a_4}\right]_{a_3=0} \tag{20}$$

$$\frac{b_1}{a_3+a_4} = \left[\frac{b_3}{a_3+a_4}\right]_{a_4=0} + \left[\frac{b_3}{a_3+a_4}\right]_{a_3=0} \tag{21}$$

$$\frac{a_1}{a_3+a_4} = \left[\frac{C\cdot a_3}{a_3} + \frac{b_4}{a_3}\right]_{a_4=0} + \left[\frac{b_4}{a_4}\right]_{a_3=0} = C + S_{43} + S_{44} \tag{22}$$

$$\frac{b_1}{a_3+a_4} = \left[\frac{b_3}{a_3}\right]_{a_4=0} + \left[\frac{b_3}{a_4}\right]_{a_3=0} = S_{33} + S_{34} \tag{23}$$

$$\Gamma_1 = \frac{b_1}{a_1} = \frac{S_{33} + S_{34}}{C + S_{43} + S_{44}} \tag{24}$$

$$\Gamma_2 = \frac{b_2}{a_2} = \frac{S_{43} + S_{44}}{C + S_{33} + S_{34}} \tag{25}$$

Figure 10 shows a test circuit with an implementation of the above technique. The top circuit consists of three amplification blocks with an in-situ probe placed at the input and output of the middle amplification block. The bottom circuits provide reference circuits to compare the reflection coefficients calculated by the in-situ calculations to a direct measurement of the same quantity. These test circuits do not contain any feedback paths, so the bisection of the circuit for the control simulations remains valid. This type of verification technique was chosen due to it's simplicity. Included in the circuit diagram are the equations used to calculate the in-situ reflection coefficients. Figure 11 shows the simulation results of the example circuit. The red traces with circles are the values obtained from the control circuits and represent the desired result. The blue traces with crosses represent the quantities calculated using the in-situ probes. It can be seen that the two techniques provide the same result.

The technique derived in this section for obtaining in-situ reflection coefficients at a circuit interface provides the same basic information as the probe previously discussed in section 3.2.1. The primary improvement is that it only requires the addition of two additional S-parameter ports to the simulation for each interface being analyzed. A secondary benefit is that when multiple in-situ probes are placed into the circuit additional information about the circuit can be obtained. The techniques required for this well be discussed in the following sections.

3.2.3 2 Port DUT

The desire for this analysis is to be able to obtain the full 2-Port S-Matrix of a sub-circuit within a larger circuit without having to deconstruct the circuit to do so. An illustration of this is shown in Figure 12. The circuit consists of three separate 2-port networks cascaded in series to form a single composite 2-port network. The S-Parameters of the cascaded

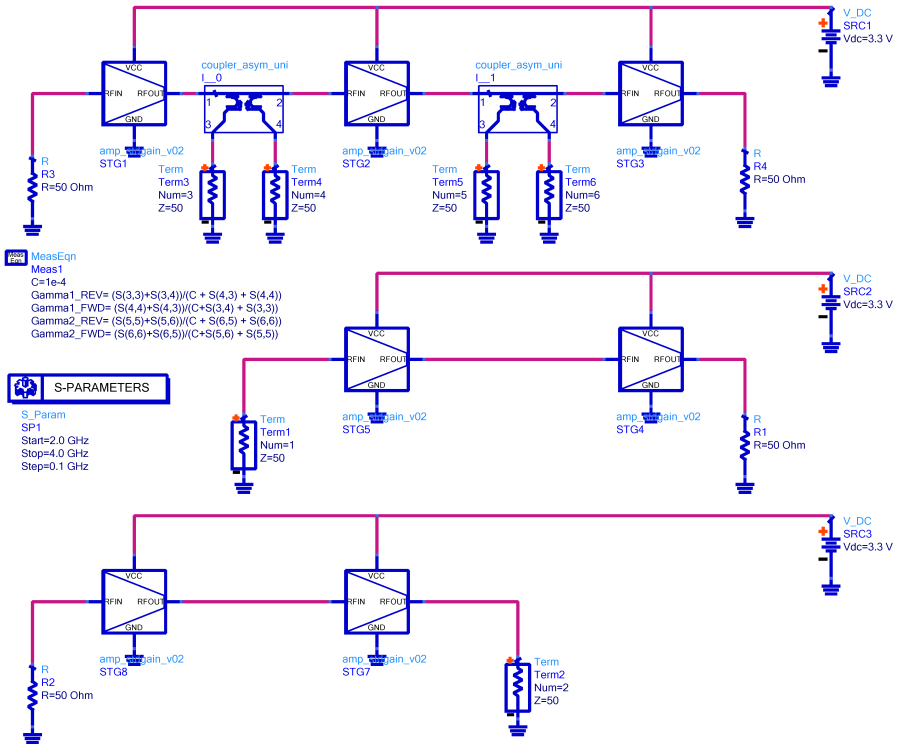

Figure 10: Schematic of test circuit for coupler based in-situ probe

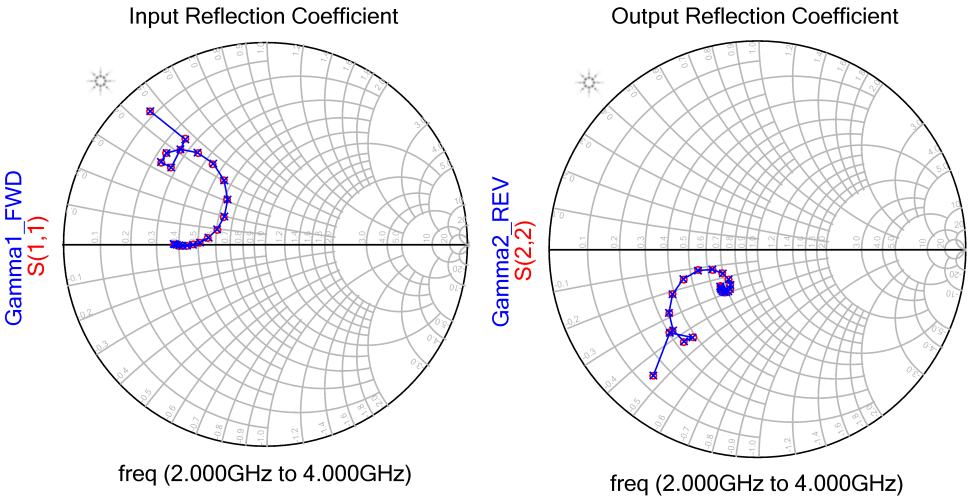

Figure 11: Plots of baseline S-Parameters and in-situ derived S-Parameters

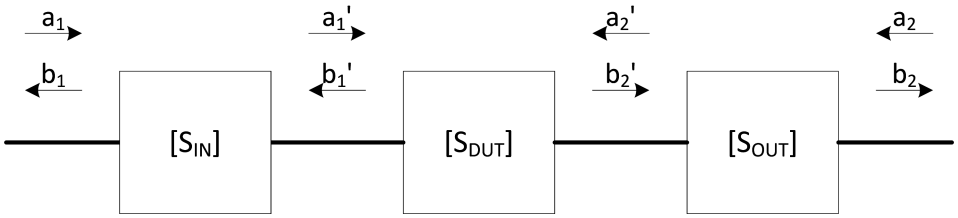

Figure 12: Diagram illustrating a two-port network under analysis being surrounded by other networks.

networks can readily be determined by measuring or simulating at the two external ports. Of particular interest are the S-Parameters of the middle network represented as S_{DUT}. Based on the theory of S-Parameters, and the primed quantities in Figure 12, S_{DUT} is known to be:

$$S_{DUT} = \begin{bmatrix} \frac{b_1'}{a_1'} & \frac{b_1'}{a_2'} \\ \frac{b_1'}{a_2'} & \frac{b_2'}{a_2'} \end{bmatrix}$$

These wave quantities are located internal to the circuit and are not readily available through traditional analysis. Simple voltage and current probing is insufficient to obtain the individual forward and reverse waves at an interface. The first challenge is to devise a means to accurately obtain information about the internal waves without perturbing the normal operational characteristics of the circuit. The second challenge is to take into account the fact that the ports of the internal network are no longer matched. This means that there could be additional reflected waves incident on the non-excitation ports. This results in there effectively being more than one simultaneous excitation. This leads to the requirement of additional terms being necessary in the resulting equations.

The approach used in this case to obtain these wave quantities is the same as used in section 3.2.2. In this case two in-situ probes are used. One is placed at the input port of S_{DUT} and the other is placed at the output port of S_{DUT}. A test-bench setup implementing this technique is shown in Figure 13. This figure shows the simple example of Figure 12 with the addition of two directional couplers at the input and output ports of the internal network. There are now 6 ports in this configuration. Ports 1 and 2 are the input and output ports of the original circuit. Port 3 is configured to sample the incident wave at the input interface of

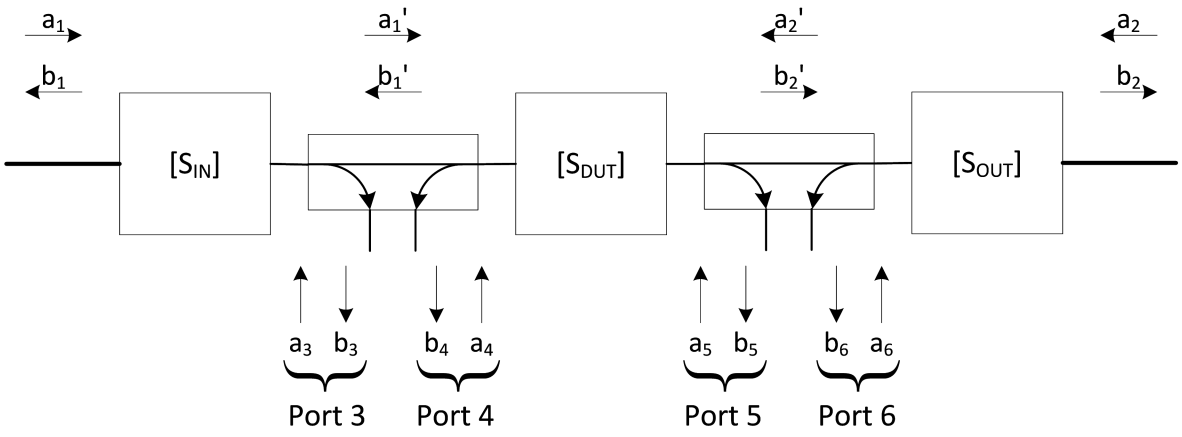

Figure 13: Diagram showing in-situ probes inserted to facilitate analysis of inner two-port network.

the internal network and Port 4 is configured to sample the reflected wave at that interface. Port 6 samples the incident wave at the output interface and Port 5 samples the reflected wave at that interface. It should be noted that the constituent parts of this setup are the same as that were used in Section 3.2.2 for the single in-situ probe. In this application two probes are used on either side of S_{DUT}. The directional coupler used for these probes is the same model as was used before and is described by S-matrix 17.

Equations 26 and 27 represent the relationship among the wave quantities of a linear 2-port network. In classical S-Parameter analysis the 2-port S-Parameters are determined by applying an excitation to one of the ports while applying a matched load to the other port. Because matched loads are used, Equations 26 and 27 become trivial to solve. When determining S_{11}, the S_{12} term disappears because a_2 is forced to zero. And likewise when determining S_{12}, the S_{11} term disappears because a_1 is forced to zero.

$$b'_1 = S'_{11} \cdot a'_1 + S'_{12} \cdot a'_2 \tag{26}$$

$$b'_2 = S'_{21} \cdot a'_1 + S'_{22} \cdot a'_2 \tag{27}$$

However, during in-situ S-Parameter analysis it is not possible to control the load conditions at each of the virtual-ports. Since the measurement is being made in-situ the effective port impedances are what they are and cannot be changed. This complicates the matter of

solving Equations 26 and 27. Because a matched load cannot be assumed at each port, both terms of each equation must be considered simultaneously. At first glance this would seem to create a system of two equations and four unknowns, thus preventing a solution. But as it turns out, there are multiple ways to obtain the virtual wave quantities a'_1 and a'_2.

$$a'_1 = C \cdot a_4 + b_3 \text{ (Port 4 Excitation)}$$

$$a'_1 = b_3 \text{ (Port 5 Excitation)}$$

$$a'_2 = C \cdot a_5 + b_6 \text{ (Port 4 Excitation)}$$

$$a'_2 = b_6 \text{(Port 5 Excitation)}$$

By using each of these methods of obtaining a'_1 and a'_2, Equations 26 and 27 can now be expanded into a system of four equations as seen in Equations 28, 29, 30, and 31.

$$b_4 = S'_{11}(C \cdot a_4 + b_3) + S'_{12}(b_6) \tag{28}$$

$$b_4 = S'_{11}(b_3) + S'_{12}(C \cdot a_5 + b_6) \tag{29}$$

$$b_5 = S'_{21}(C \cdot a_4 + b_3) + S'_{22}(b_6) \tag{30}$$

$$b_5 = S'_{21}(b_3) + S'_{22}(C \cdot a_5 + b_6) \tag{31}$$

By moving all of the wave quantities in Equations 28 through 31 to the right-hand side, the system can now be re-written as:

$$1 = S'_{11}\left(C \cdot \frac{a_4}{b_4} + \frac{b_3}{b_4}\right) + S'_{12}\left(\frac{b_6}{b_4}\right)$$

$$1 = S'_{11}\left(\frac{b_3}{b_4}\right) + S'_{12}\left(C \cdot \frac{a_5}{b_4} + \frac{b_6}{b_4}\right)$$

$$1 = S'_{21}\left(C \cdot \frac{a_4}{b_5} + \frac{b_3}{b_5}\right) + S'_{22}\left(\frac{b_6}{b_5}\right)$$

$$1 = S'_{21}\left(\frac{b_3}{b_5}\right) + S'_{22}\left(C \cdot \frac{a_5}{b_5} + \frac{b_6}{b_5}\right)$$

Another substitution has to be made at this point. This is because linear S-Parameter simulations do no provide direct access to the wave quantities of the circuit. In order to make practical use of these equations the wave quantities must be replaced with quantities that are available in the S-Parameter simulation results. It turns out that all of the ratios on the system can be represented by ratios of S-Parameters. This is by light of the fact that $\frac{b_3}{b_4} = \frac{b_3/a_4}{b_4/a_4} = \frac{S_{34}}{S_{44}}$. During this substitution all of the S-Parameters in any given equation must be use the same excitation port. Otherwise the S-Parameters are not actually related to each other and can yield incorrect results.

$$1 = S'_{11}\left(C \cdot \frac{1}{S_{44}} + \frac{S_{34}}{S_{44}}\right) + S'_{12}\left(\frac{S_{64}}{S_{44}}\right)$$

$$1 = S'_{11}\left(\frac{S_{35}}{S_{45}}\right) + S'_{12}\left(C \cdot \frac{1}{S_{45}} + \frac{S_{65}}{S_{45}}\right)$$

$$1 = S'_{21}\left(C \cdot \frac{1}{S_{54}} + \frac{S_{35}}{S_{54}}\right) + S'_{22}\left(\frac{S_{65}}{S_{54}}\right)$$

$$1 = S'_{21}\left(\frac{S_{35}}{S_{55}}\right) + S'_{22}\left(C \cdot \frac{1}{S_{55}} + \frac{S_{65}}{S_{55}}\right)$$

When the above system of equations is solved the S Matrix of the DUT with matched terminations at both ports is obtained. The resulting equations are shown in Equations 32 through 36.

$$\delta_{DUT} = (C + S_{34})(C + S_{65}) - S_{35}S_{64} \tag{32}$$

$$S'_{11} = \frac{S_{44}(C + S_{65}) - S_{45}S_{64}}{\delta_{DUT}} \tag{33}$$

$$S'_{12} = \frac{S_{45}(C + S_{34}) - S_{44}S_{35}}{\delta_{DUT}} \tag{34}$$

$$S'_{21} = \frac{S_{54}(C + S_{65}) - S_{55}S_{64}}{\delta_{DUT}} \tag{35}$$

$$S'_{22} = \frac{S_{55}(C + S_{34}) - S_{54}S_{35}}{\delta_{DUT}} \tag{36}$$

A simulation testbench implementing this approach is shown in Figure 14. This test bench contains two circuits under analysis. The top most circuit connected to analysis ports 1 and 2 is a single amplification stage matched to 50 ohms at the input and output. The contents of this circuit component are not needed as it is simply here to represent a two-port amplifier stage. This block represents the two-port network that will be extracted in-situ and will be referred to as the DUT. The bottom circuit contains the same DUT amplifier block with an additional two-port network cascaded on both sides of it. These additional two-port blocks are arbitrary and intended to represent the networks surrounding the DUT. In addition a feedback loop has been placed around the entire circuit. An in-situ probe has been placed at both the interface between the input network and the input port of the DUT and the output port of the DUT and the output network. These are the in-situ probes that will be used to extract the two-port S-Parameters of the DUT in-situ.

The in-situ probes in the bottom circuit utilize analysis ports 3 through 6. These port numbers correspond with the designations used during the derivation of Equations 32 through 36. The implementation of these equations in the simulation is shown with the schematic. Figure 15 shows the simulations results. The four terms of the resulting S-matrices are shown with the baseline results plotted with the in-situ results. The baseline results are designated by the o markers, and the in-situ results are designated by the x markers. It can be seen that the results are identical.

3.2.4 2 Port Loop

The analysis described in this section is a hybrid of the approaches shown in Sections 3.2.2 and 3.2.3. The objective is to extend the analysis in section 3.2.2 to include the coupling between the

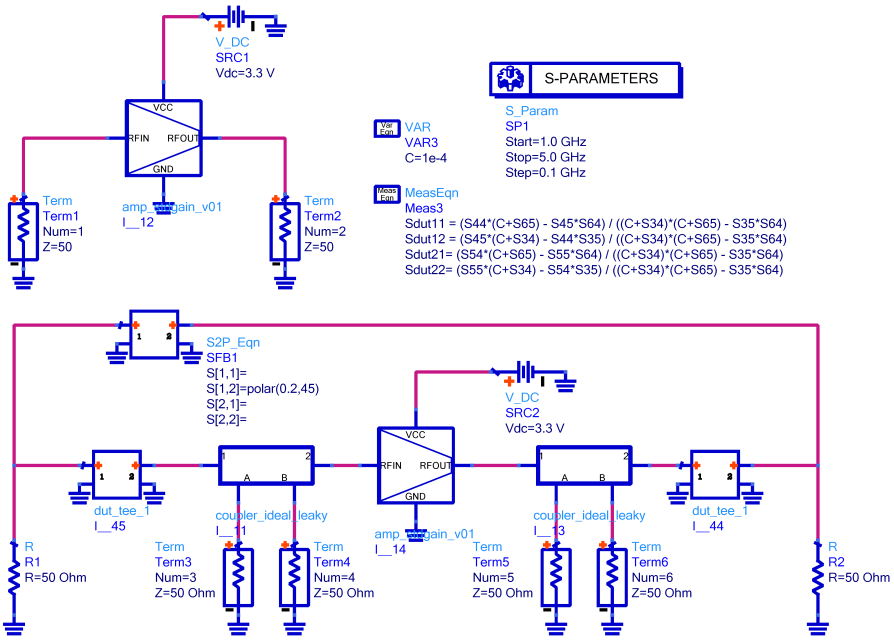

Figure 14: Schematic of ADS test circuit for 2-Port DUT in-situ probe.

forward and reverse ports. This will result in a 2-port S-Matrix representation of the coupling between these ports. For the purposes of the analysis in this section Port 1 of the S-Matrix will be chosen to represent the forward port and Port 2 will be chosen to represent the reverse port. The $S_{11}$and S_{22}terms of the resulting S-matrix matrix will correspond with the reflection coefficients of ports 1 and 2 when a matched condition is placed on the opposing port. The S_{12} and S_{21} terms will correspond to the coupling between Ports 1 and 2 in the forward and reverse direction respectively.

For now the network under analysis will be considered as a black box, as shown in Figure 16. An example is to consider the circuit of Figure 4. If the in-situ probe was inserted into the network at the connection between S_{IN} and S_{DUT} the entire circuit could be reduced into a single 2-port network as shown in Figure 4. The problem is how to determine all four parameters of the full 2-port S-Matrix using a single in-situ probe. This is done in a similar manner to the derivation in Section 3.2.3.

There are four parameters that will need to be obtained, which means that a system of four equations must be constructed. This can be done by defining the incident and

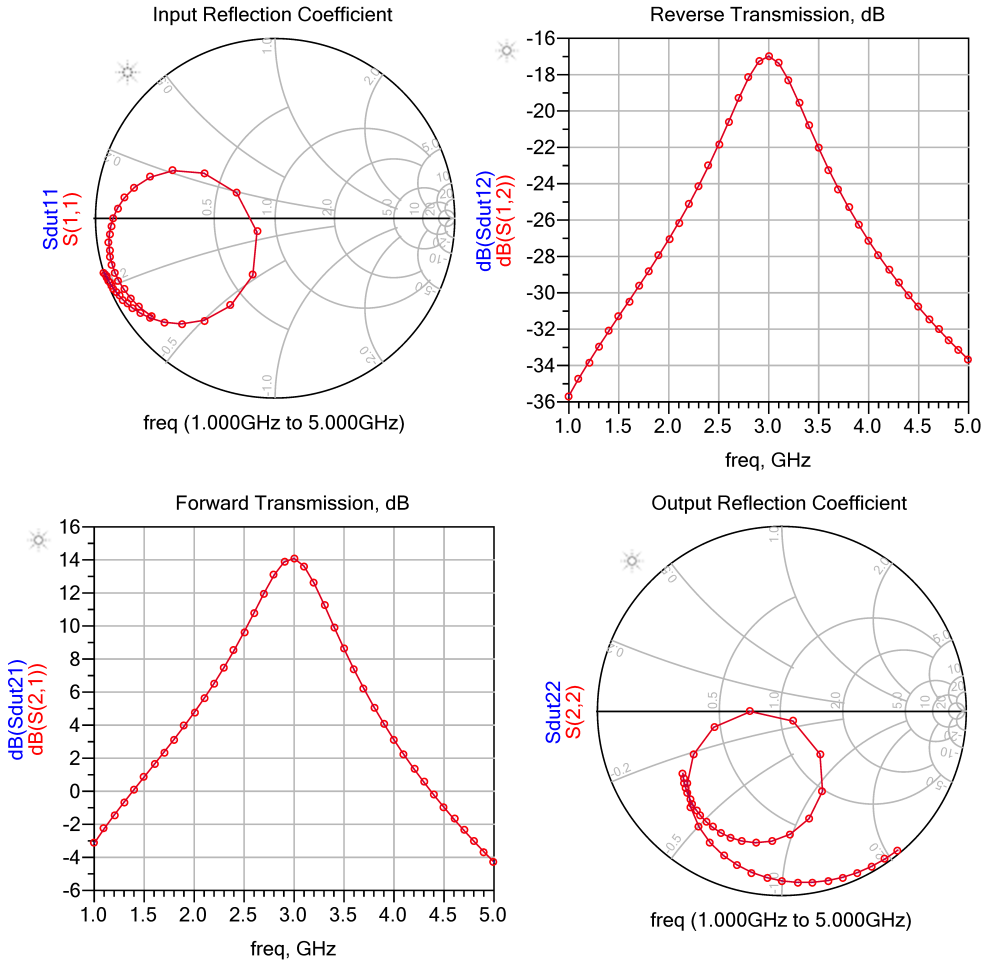

Figure 15: Plots of baseline S-Parameters and in-situ derived S-Parameters of two-port network.

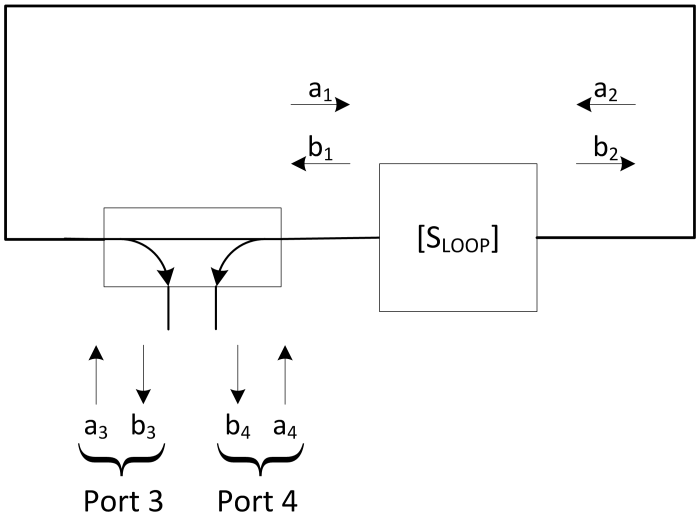

Figure 16: Diagram showing in-situ probe connected to both ports of a two-port network.

reflected wave quantities as a result of two different exciting sources as shown in the system of Equations 37 through 40. These expressions are very similar to those used in section 3.2.3, and the process of solving the resulting system of equations is similar as well.

$$a_1 = b_1 \text{ (Port 3 Excitation)}$$

$$a_1 = C \cdot a_4 + b_1 \text{ (Port 4 Excitation)}$$

$$a_2 = C \cdot a_3 + b_2 \text{ (Port 3 Excitation)}$$

$$a_2 = b_2 \text{ (Port 4 Excitation)}$$

$$b_3 = S_{22}(C \cdot a_3 + b_4) + S_{21}(b_3) \tag{37}$$

$$b_4 = S_{12}(C \cdot a_3 + b_4) + S_{11}(b_3) \tag{38}$$

$$b_3 = S_{22}(b_4) + S_{21}(C \cdot a_4 + b_3) \tag{39}$$

$$b_4 = S_{12}(b_4) + S_{22}(C \cdot a_4 + b_3) \tag{40}$$

This system of equations is solved in the same manner as before. The solution is described by Equations 41 through 45.

$$\delta_{LOOP} = (C + S_{34})(C + S_{43}) - S_{33} \cdot S_{44} \tag{41}$$

$$S_{11} = \frac{C \cdot S_{44}}{\delta_{LOOP}} \tag{42}$$

$$S_{12} = 1 - \frac{C \cdot (C + S_{34})}{\delta_{LOOP}} \tag{43}$$

$$S_{21} = 1 - \frac{C \cdot (C + S_{43})}{\delta_{LOOP}} \tag{44}$$

$$S_{22} = \frac{C \cdot S_{33}}{\delta_{LOOP}} \tag{45}$$

$$S_{LOOP} = \begin{bmatrix} \frac{C \cdot S_{44}}{\delta_{LOOP}} & 1 - \frac{C \cdot (C + S_{34})}{\delta_{LOOP}} \\ 1 - \frac{C \cdot (C + S_{43})}{\delta_{LOOP}} & C \cdot S_{33} \end{bmatrix}$$

Note that Equations 41 through 45 return the unloaded S-matrix of the surrounding circuit. This is analogous to the situation created in the bottom circuit of Figure 4. As such the $S_{11}$and S_{22} terms are not equivalent to the reflection coefficients 24 and 25 obtained in Section 3.2.2.

A simulation testbench implementing this in-situ analysis is shown in Figure 17. The top circuit in the figure represents a passive circuit. Again the detail of this circuit are not of particular interest. The only concern is whether the in-situ analysis returns the same results. The bottom circuit consists of the same passive network with an in-situ probe connected between the network's two ports. The input of the in-situ probe is connected to port 2 of the passive network and the output port of the in-situ probe is connected to port 1 of the passive network. This is done to maintain consistency with the convention established for the derivation of Equations 41 through 45 and with Figure 16. The S-Parameter analysis ports also correspond to the convention used during the derivation.

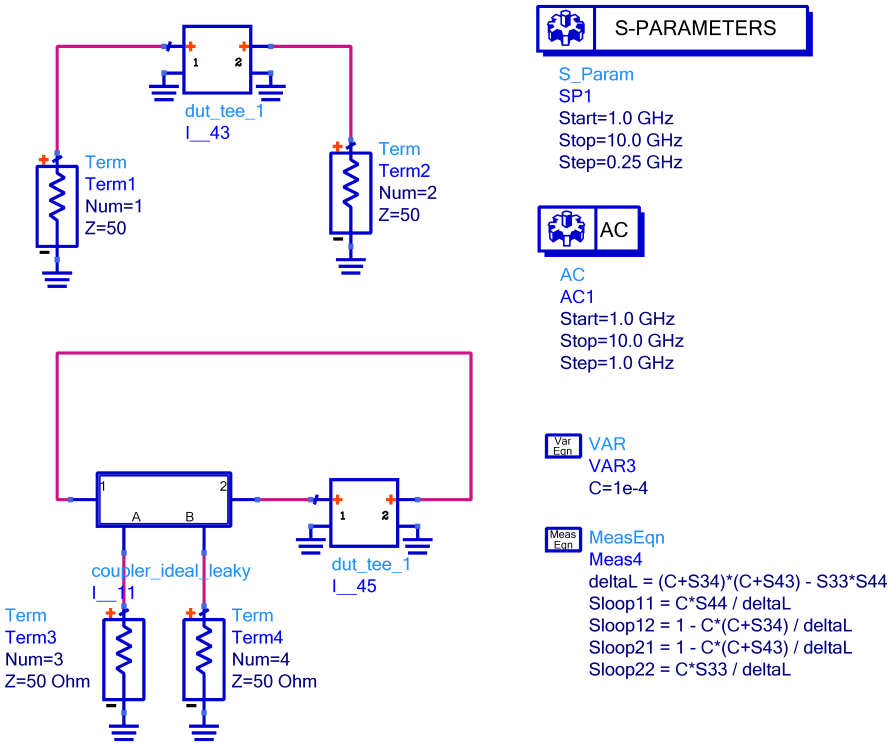

Figure 17: Schematic of test circuit for 2-Port loop in-situ probe

Figure 18 shows the simulation results plotted in the polar domain. The S-Parameters of the top circuit are designated by the o markers and the S-Parameters of the in-situ analysis are represented by the x markers. It can be seen that the S-Parameters returned by both analysis techniques are identical.

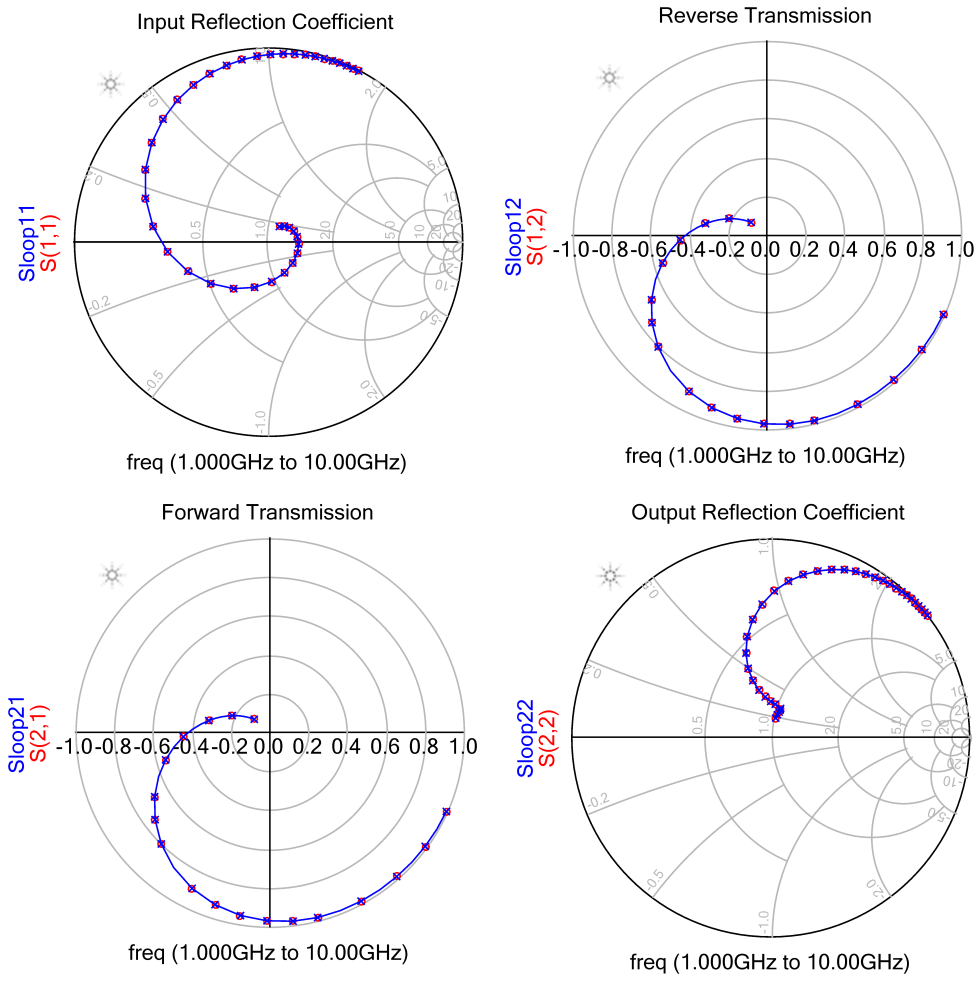

Figure 18: Plots of baseline loop S-Parameters and in-situ derived loop S-Parameters.

Chapter IV

APPLICATION OF IN-SITU PROBES

This section will cover various applications for the use of in-situ probes. These applications will focus on multi-stage amplifier design, however useful applications are not limited to only this type of design. The primary use that will be investigated is for stability analysis and the impact that marginal stability may have on the overall gain of the circuit under analysis.

4.1 Stability Criteria

There are two directions from which the subject of stability can approached. One approach is to derive and understand the necessary and sufficient conditions for an oscillation to exist. This is the approach generally seen and used for oscillator design. It allows the designer to understand the necessary conditions that must be met in order for any oscillator design to be successful. The other approach is to derive and understand the necessary and sufficient conditions to guarantee that under no circumstances can a network sustain an oscillation. This is the approach generally taught and used for amplifier circuit design. These two approaches serve to define the boundaries of active circuit stability analysis. On one side an oscillation is guaranteed, and on the other side the absence of oscillation is guaranteed.

This discussion will focus on the region of active circuit stability analysis that exists between these boundaries. The region of potential instability, but with margin. It is important that a designer be able to derive, measure, and interpret additional figures of merit that allow them to judge how much margin, and the impact on the overall circuit behavior caused by potential instabilities.

4.1.1 Oscillator Condition

The necessary and sufficient conditions for oscillation discussed in this section are derived with the assumption that a negative resistance model is being used to represent the active

circuit in question. This analysis approach and model yields itself quite well to the types of modeling techniques used in RF / microwave circuit analysis, and in particular to the values returned from the type of in-situ probes discussed in earlier sections. There are two primary components to a negative-resistance model. First is the active device that is capable of adding energy into the system, and is modeled as a resistance with a negative value. The negative resistance implies that the component is generating energy rather than dissipating it. Second is a resonant circuit that is connected to the negative resistance. An example circuit is shown in Figure 19. The tuned resonator provides the energy storage components necessary for sustained oscillation. For the typical amplifier design the resonant circuit generally consists of an inductive network and a capacitive network. The resonant frequency of this network, defined as the frequency at which the reactance of the inductive and capacitive portions are equal and opposite, corresponds to the frequency at which the network can support sustained osculation. This is a result of the phase shift of the loop-gain equation crossing the zero axis as described in [4].

With these components, the model can be described as being capable of generating an oscillation, but the question of whether an oscillation can be sustained still remains. There are three possible characteristics for the behavior of this model if it is perturbed: increasing signal amplitude, constant signal amplitude, and decreasing signal amplitude. Which of these three possibilities that actually occurs is determined by the non-reactive components present in the resonant circuit. If the net impedance of all the real (resistive) components in a circuit is positive, then the amplitude of oscillation will decrease with increasing time until the oscillation dies out. The more net positive the impedance is the faster the oscillation will die out. Conversely, if the net real impedance is negative, the oscillation amplitude will increase with increasing time. The more net negative the impedance the faster the amplitude will grow. If the network is completely loss-less resulting from the net real component being zero, the amplitude of the oscillation will remain constant. The condition of zero net resistance is the only condition under which sustained oscillations can exist.

It is implied from the descriptions above that in order for a circuit to be a successful oscillator it must be able to modulate the effective real impedance connected to the resonator.

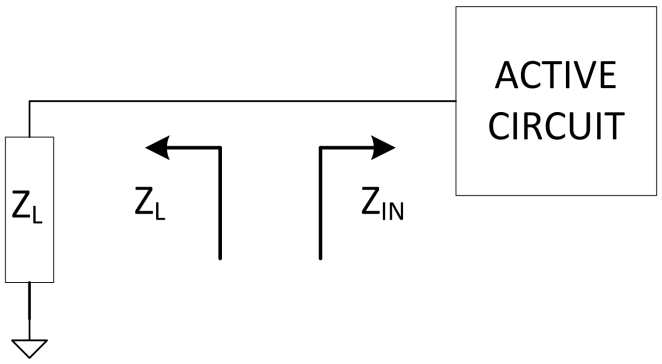

Figure 19: Block diagram of negative resistance oscillator

When properly implemented this enables the oscillator to allow the oscillation to grow to an appropriate amplitude and then remain at a constant amplitude. This is only possible by modulating the real impedance as a function of signal amplitude. At low signal amplitudes the net resistance should be negative causing the signal strength to build. As the signal strength approaches the desired value the net resistance of the circuit will approach zero. This results in the oscillation amplitude building to a desired level and then being maintained at a constant level. Otherwise the oscillation will either die out or result in clipping the circuit.

These conditions are described and captured in [4] with a compact set of equations. These equations are referenced to a single-port active network with a passive load connected directly to the active networks singular port as shown in Figure 19. The impedance / admittance seen looking into the active network is described as Z_{IN} or Y_{IN} respectively, and the impedance / admittance of the passive network is described as Z_L or Y_L respectively. Equations 46 are for series tuned circuits, and Equations 47 are for parallel tuned circuits. It is important to ensure that the appropriate set of equations is being used for a particular circuit as incorrect results will otherwise be obtained. It is therefore important to ensure that the specific tuning (series or parallel) of a network is known so that the appropriate equations can be applied.

$$Z_{IN}(A_0, \omega_0) + Z_L(\omega_0) = 0 \tag{46}$$
$$Re(Z_{IN} + Z_L) = 0$$
$$Im(Z_{IN} + Z_L) = 0$$

$$Y_{IN}(A_0, \omega_0) + Y_L(\omega_0) = 0 \tag{47}$$
$$Re(Y_{IN} + Y_L) = 0$$
$$Im(Y_{IN} + Y_L) = 0$$

When the conditions of Equations 46 or 47 are satisfied the circuit is capable of sustaining steady-state oscillations. Note that there is only one condition under which this occurs when both the real and imaginary components of the combined impedance / admittance equal zero. If either of these conditions is not net then sustained oscillations cannot exist. This does not mean that the circuit is what would be typically be considered stable. Under conditions where either or both of the real and imaginary components approach the oscillatory conditions the circuit will exhibit ringing when excited at that frequency. The close the conditions are the longer the ringing will take to decay. Thus circuits which contain nodes that approach the oscillatory condition will exhibit ringing in the time domain and gain peaking in the frequency domain. These effects will be examined in more detail in the following sections.

The requirement of the above criteria to know whether the networks on both sides of the reflection plane are parallel or series tuned can sometimes be a significant burden. Often times one is not sure exactly which tuning the circuit is exhibiting and an assumption must be made upon inflections as observed on a Smith chart. This prevents a universal methodology from being used. Equation 48 shows a formulation of the above criteria that is universally applicable to both parallel and series tuned circuits. It is able to achieve this ability by being derived using reflection coefficients as opposed to impedance or admittance. This is a result of reflection coefficients being able to universally describe the behavior of a

network without needing to know it's schematic representation. It can be shown that this formulation is equivalent to those shown in 46 and 47[4]. When the quantity defined in Equation 48 is equal to unity the circuit is capable of sustaining steady state oscillations. In this case unity is defined as having a magnitude of strictly one and a phase of strictly zero. If the magnitude is greater than one, then any oscillation will build in amplitude, and if the magnitude is less than one then any oscillation will decay in amplitude. If the angle is not equal to zero then the circuit is incapable of sustaining oscillation at that frequency.

$$\Gamma_{IN}(\omega) \cdot \Gamma_L(\omega) = 1 + j0 \tag{48}$$

One port in-situ stability analysis is an extension of Equation 48. The model used to derive Equations 46, 47, and 48 assumes a one-port active network and a one-port passive network. To adapt this model for use with in-situ probes the assumption about the nature of each network needs to be removed, since the nature of the networks seen looking in either direction from the in-situ probe is unknown. As it turns out, no special modifications are required for this. Since the terms in the equation are symmetric it doesn't matter which sides contribute to the amplification as they both contribute equally. Thus Equation 48 can be rewritten in terms of the reflection coefficients returned from the in-situ probe derived in section 3.2.2. This is shown in Equation 49. In this case the Γ_1 and Γ_2 terms are the same as defined in Equations 24 and 25.

$$\Gamma_{TOT} = \Gamma_1 \cdot \Gamma_2 \tag{49}$$

Equation 49 can be used to quantify the stability of a circuit. The further away from unity the magnitude of Γ_{TOT} is the further away the circuit is from being able to sustain oscillations. In addition the further away the angle of Γ_{TOT} is from 0 degrees, the further away the circuit is from the oscillatory condition. Unfortunately Γ_{TOT} does not provide a good means for understanding exactly what the circuit will do. A closer examination of this question will be covered later.

4.1.2 Gain Peaking

As the conditions for oscillation discussed in the previous sections are approached circuits will begin to exhibit undesirable behavior. One such manifestation of undesirable behavior is that of gain peaking. Gain peaking will exhibit itself as a sharp rise in the forward gain of a circuit at certain frequencies. The frequencies at which this peaking occurs are those at which nodes in the circuit approach the oscillatory conditions previously discussed. If the nodes fully satisfy the conditions for oscillation it is mathematically possible for the gain to approach infinity. This section will investigate two models under which gain peaking can arise. The first is a loop gain model where an explicit feedback loop is the origin of the instability. The second is the result of greater than unity reflections caused by negative resistances being generated by a circuit component.

4.1.2.1 Loop Gain

The quantities derived in Section 3.2.4 are applicable for use in analyzing feedback loops within a network. Of particular interest when analyzing feedback loops is the loop gain quantity $A\beta$. This is a vector quantity the represents the amount of signal present at the summation node relative to the original input signal. In the case examined in Section 3.2.4 the summation node is the node at which the in-situ probe is placed. The original signal is that incident on port 1 and the feedback signal is the signal emerging from port 2. This is illustrated in the signal flow graph shown in Figure 20. This shows that there are in fact two signals that arrive at the a_1' node. The original incident signal $a_1$and a copy of the original signal scaled by $S_{LOOP,21}$. This scaled signal is the aggregate result of all the feedback loops present in the circuit. In this case the quantity $S_{LOOP,21}$ is the same as is defined in Equation 44 and is synonymous with loop gain $A\beta$. When the flow graph is reduced the resulting simplified term representing the incident wave on node a_1' is shown in Equation 50. From this equation it can be seen that as $S_{LOOP,21}$ approaches unity with zero phase the resulting signal incident on node a_1' rapidly increases in amplitude. The end result of this is that at the frequencies at which the loop-gain approaches unity the gain response of the system will begin to exhibit peaking. The closer to unity the $S_{LOOP,21}$ term

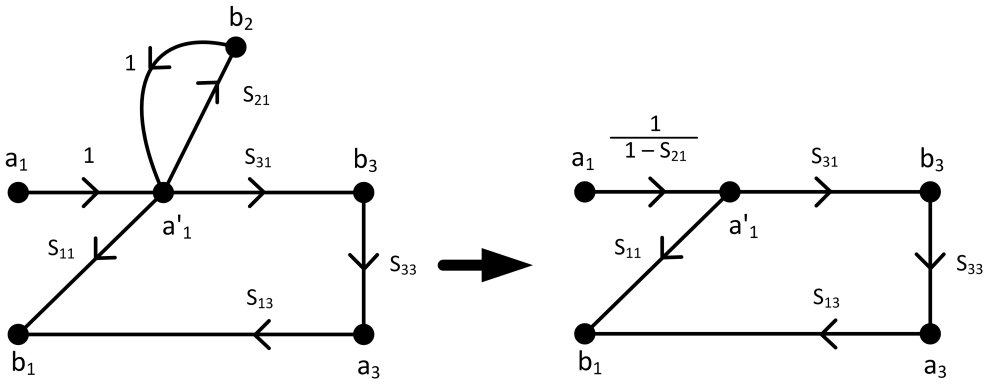

Figure 20: Signal flow graph illustrating feedback in circuit

becomes the larger the gain peak.

$$a_1' = \frac{a_1}{1 - S_{LOOP21}} \tag{50}$$

$$G_{PEAKING} = \frac{a_1'}{a_1} = \frac{1}{1 - S_{LOOP21}}$$

4.1.2.2 Reflections

The stability criteria expressed in Equation 48 is defined in such a way as to not provide much information regarding what impact there will be on circuit performance as the circuit approaches the oscillatory condition. At this point a means for quantifying the impact on overall circuit performance that a particular network interface has. To help quantify this impact a figure of merit representing the amount of potential gain peaking that could result if the node under analysis was in the direct signal path of an amplifier . This figure of merit is useful since it corresponds to overall network behavior and is intuitive to understand.

Figure 21 will be used to investigate the amount of potential gain peaking contributed by such a reflection interface. The desired result is a ratio of the signal transmitted through the interface to the signal incident upon it. In Figure 21 the transmitted signal is represented by a_{OUT} and the incident signal is represented by a_{SRC}. By examining the flow graph it can be seen that a_{OUT} is equal to b_{IN}, which is the combination of the incident signal a_{SRC} and the reflections resulting from the cascade of a_{OUT}, Γ_{OUT}, and Γ_{IN}. Therefore a_{OUT} is a

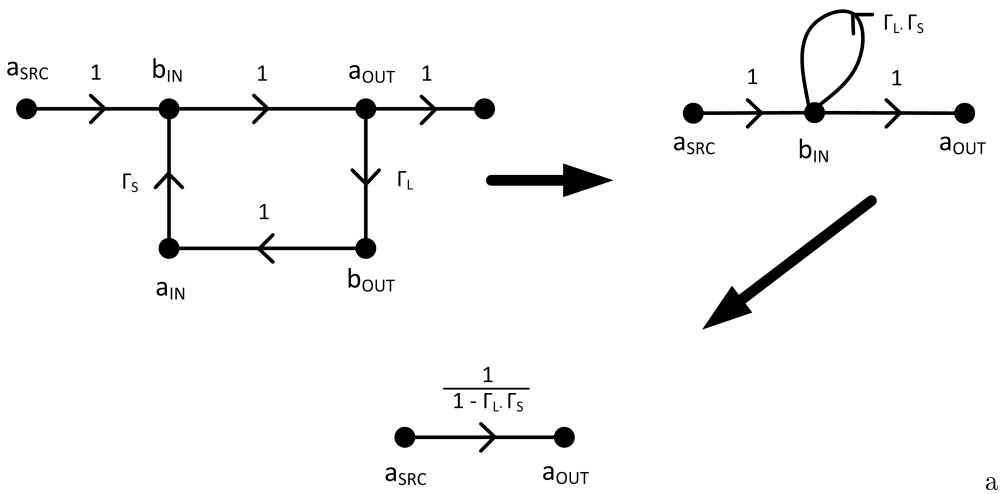

also

Figure 21: Signal flow graph of two back to back two-ports with mismatched interface

function of itself and is thus a result of a feedback loop. This is is described by Equation 51. It should be noted that Equation 51 contains the same term $\Gamma_{IN}\Gamma_{OUT}$ as was derived in 49. When this expression is rearranged in terms of gain the result is Equation 52. This shows that as the quantity Γ_{TOT} approaches unity the resulting gain peaking will increase towards infinity.

$$a_{OUT} = b_{IN} = a_{IN} + a_{OUT} \cdot \Gamma_{IN} \cdot \Gamma_{OUT} \tag{51}$$

$$a_{OUT} = \frac{a_{IN}}{1 - \Gamma_{IN} \cdot \Gamma_{OUT}} = \frac{a_{IN}}{1 - \Gamma_{TOT}}$$

$$\frac{a_{OUT}}{a_{IN}} = G_{PEAK} = \frac{1}{1 - \Gamma_{TOT}} \tag{52}$$

It is important to note that it is assumed the transmission into the reflection interface and the transmission out of the interface is unity. This yields results that may appear non-intuitive. In the situation where both networks on either side of the reflection interface are passive the transmission coefficients will not be zero. Since passive 2-port networks must be passive and reciprocal the transmission coefficients will be equal to $\sqrt{1 - |\Gamma|^2}$. This is true both for the input network and the output network. As a result the total cascaded gain of the input and output network with the effect of reflections at their interface will be as described

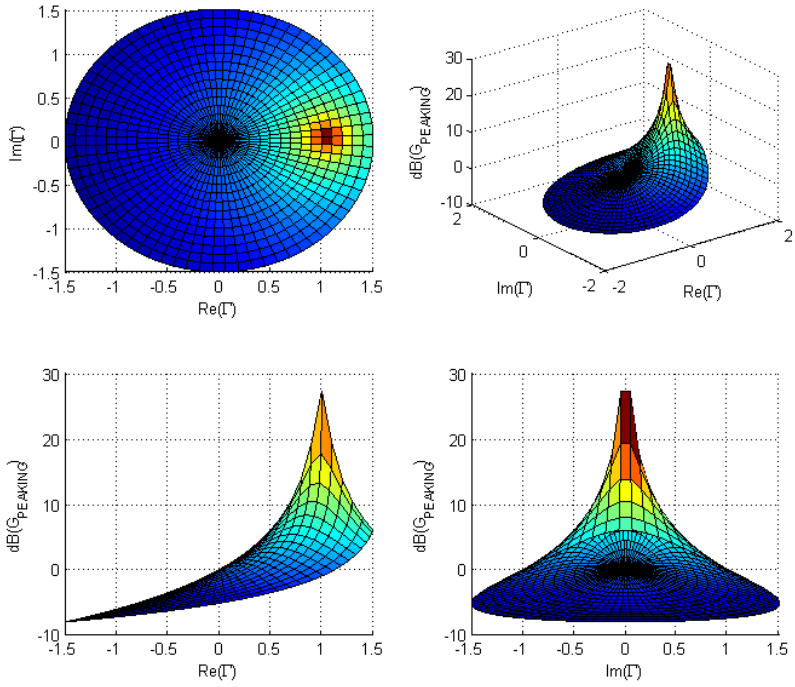

Figure 22: 3D Plot showing gain peaking as a function of Γ_{TOT}

by Equation 53. If Γ_{IN} and Γ_{OUT} are conjugates of each other the result of Equation 53 is unity. This is the condition of a perfect conjugate match between two networks, and thus results in maximum power transfer. However these terms in the numerator can no longer be assumed to be representative of the behavior of an active network. Since an active network is non-passive and is typically non-reciprocal the assumption of the transmission coefficient being $\sqrt{1-|\Gamma|^2}$ is no longer valid. As a result these coefficients have been removed from the initial equation for gain peaking shown in Equation 52.

$$G_{PEAK,PASSIVE} = \frac{\sqrt{1-|\Gamma_{IN}|^2}\cdot\sqrt{1-|\Gamma_{OUT}|^2}}{1-\Gamma_{IN}\cdot\Gamma_{OUT}} \tag{53}$$

Figure 22 provides a graphical depiction of the amount of gain peaking (in dB) predicted by Equation 52 as a function of Γ_{TOT}. This graphically illustrates that if the conditions for oscillation are approached the circuit will have a gain that rises rapidly. Figure 22 also seems to indicate that as one moves away from this condition there will still be gain peaking. This is a result of the terms in the numerator of Equation 53 being removed from Equation 52. As a

result the values depicted in Figure 22 cannot be applied directly to a circuit as they are more an indication of the relative impact of the reflections to the circuit. A proposed solution is to pick the reflection coefficient that has the lowest magnitude and use it as the normalization coefficient for both terms in the numerator resulting in Equation 54. The assumption is that one out of the two networks is passive and will likely yield the reflection coefficient with the smallest magnitude. The benefit is that the resulting equation is normalized for reflection losses and may yield a more intuitive result.

$$G_{PEAK,NORMALIZED} = \frac{1 - min\left(|\Gamma_{IN}|^2, |\Gamma_{OUT}|^2\right)}{1 - \Gamma_{IN} \cdot \Gamma_{OUT}} \tag{54}$$

4.2 Application Example

To illustrate the application of some of the key analysis techniques developed in previous sections their application to a multi-stage amplifier design will be examined. Figure 23 presents an ADS schematic of a 3-stage PA design as it might exist just after all the individual components were brought together for the first time. In this example it is assumed that the individual components have shown stable behavior when they were initially developed. This example will show that a serious problem exists within the composite design even though the apparent performance as observed from the simulation input and output ports seems reasonable.

Figure 24 contains plots of the typical small signal parameters that would be used to analyze an amplifier. These are the simulation results obtained using the external S-Parameter analysis ports 1 and 2 as shown in Figure 23. These plots consist of S_{11} and S_{22} on both rectangular and Smith charts, and S_{21} plotted in dB. Both the Rollet's k-factor and Mu stability criteria have been calculated and are plotted. The amplifier appears to be stable based on both stability criteria being met across the band. The input match looks reasonable, amplifier gain is a bit high, and the output match needs improvement. These observations suggest that only minor adjustments and corrections to the design would be necessary, but they fail to reveal that a stability problem may exist within the design.

Figure 25 shows the in-situ S-parameters obtained at the input and output of each active

stage from the in-situ probes seen in the schematic of Figure 23. Plots labeled with REV are of the impedance seen looking from the probe towards the input of the amplifier. The plots labeled FWD are the impedance seen looking from the probe towards the output of the amplifier. These plots show that most of the networks are presenting passive terminations with the exception of the output of the second stage. The Smith Chart labeled 'Stage 2 - OUT REV' is showing a reflection coefficient that has a magnitude significantly larger than one. The polar plot labeled 'Stage 2 - OUT TOTAL' is a plot of Equation 49 applied to the in-situ parameters measured at the output of the second stage. This graph shows that Γ_{TOT} has a magnitude greater than unity over a wide range of frequencies. This indicates that the circuit is generating a net negative resistance at this node and is primed for oscillation and ringing. The angle of Γ_{TOT} never experiences a zero-crossing indicating the conditions for sustained oscillation are not satisfied. As a result the design is not currently exhibiting an oscillatory condition but will likely exhibit strong ringing in the time domain impulse response and gain peaking in the frequency domain.

The information provided by the in-situ probes clearly shows that a problem exists in the design involving the output node of the second stage. By placing in-situ probes at the input and output of each stage this observation is straightforward and the location of the problem is clear. In this case the likely cause of the potential instability at the output of the second stage is the shared ground connection between the second and third stages. This shared connection is creating a feedback path from the third stage back into the second stage. If in-situ probes had not been implemented in the design process this problem may have never been found. Failure to identify the problem during the early design stage could result in anomalous behavior during the following design stages, or it could ultimately result in a fabricated amplifier that misbehaves catastrophically in the lab.

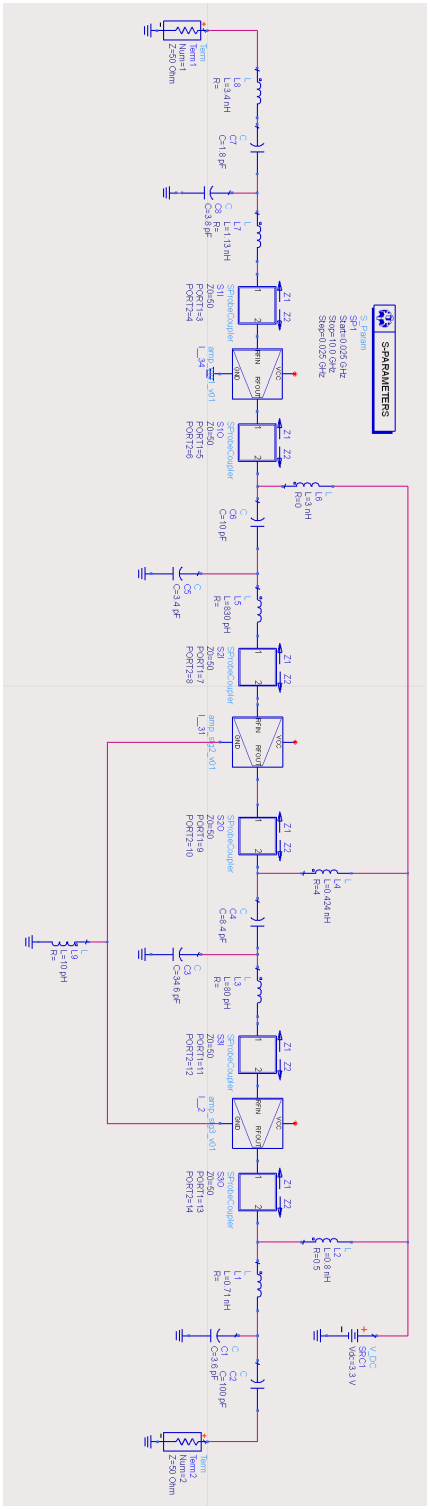

Figure 23: Schematic of a three stage power amplifier with stability issues

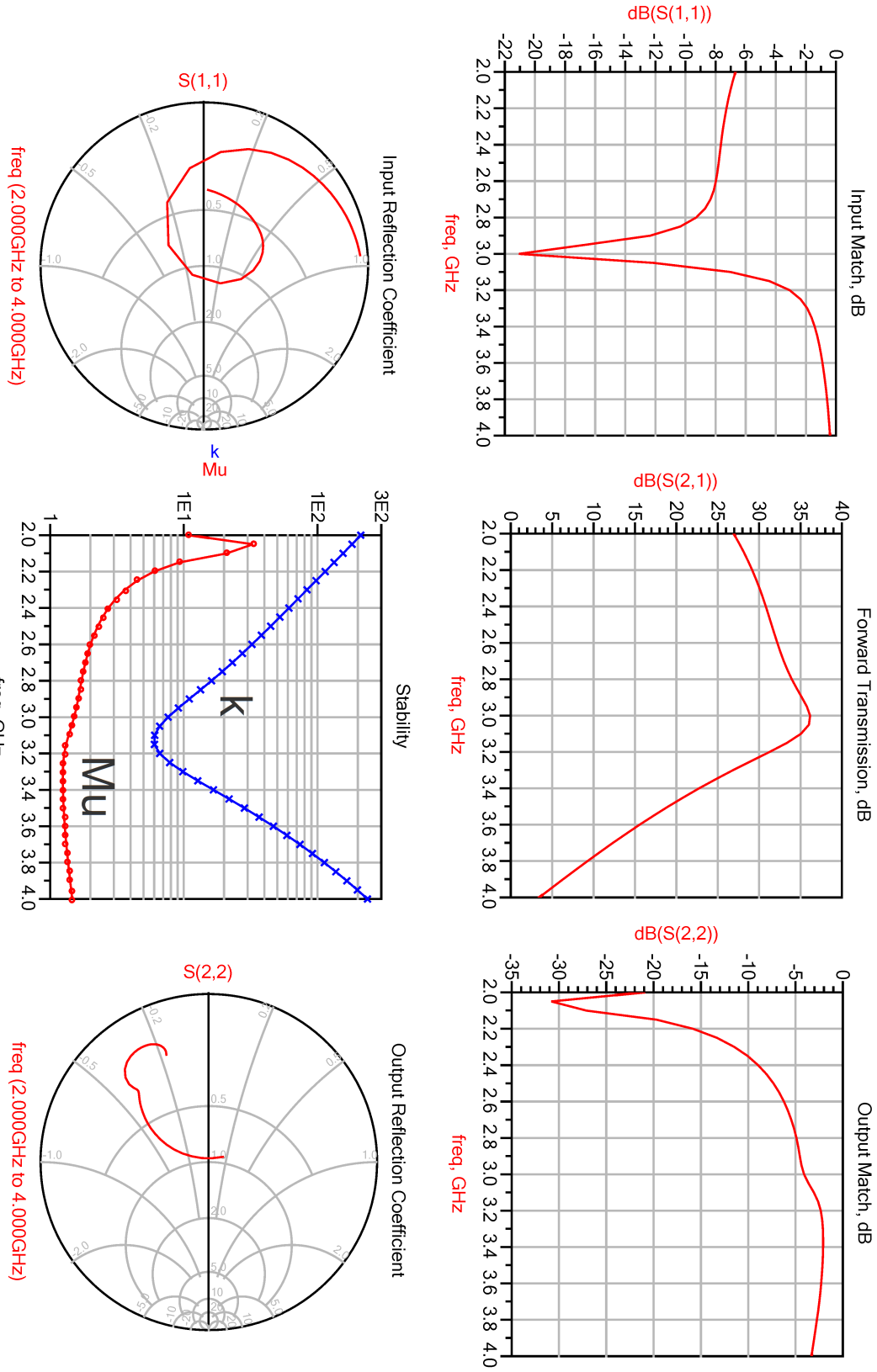

Figure 24: Graphs showing results of traditional amplifier and stability analysis

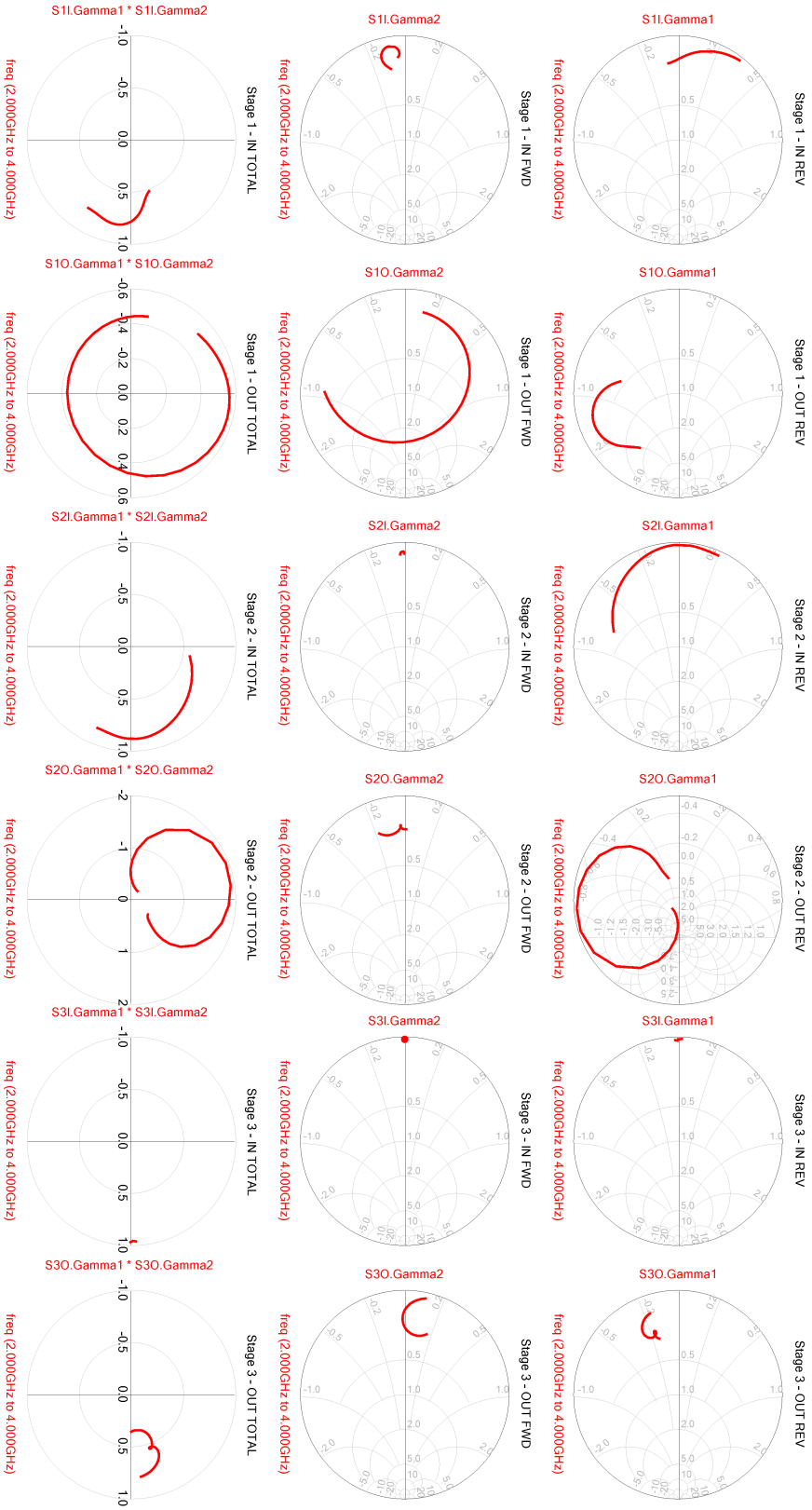

Figure 25: Graphs showing results of in-situ stability analysis on three stage power amplifier

Chapter V

CONCLUSION

An examination into various techniques for obtaining S-Parameters at circuit interfaces in-situ has been presented. The requirements for accurately obtaining these parameters while not perturbing the natural operating characteristics of the circuit have been discussed. Each of these methods has its tradeoffs, but in general the coupler based approaches yield more complete information and require the least amount of simulation resources.

The information gathered using the in-situ techniques presented can be used to better understand the underlying behavior of RF networks. Several approaches for interpreting the resultant quantities have been investigated. By implementing the in-situ techniques presented here, a circuit designer can more readily determine if the behaviors of a circuit are acceptable. Moreover, if the behaviors are deemed unacceptable, the techniques presented provide a superior means for identifying the location and nature of the problem. Therefore, the additional information provided through this approach makes the task of identifying and resolving potential stability issues considerably easier.

The multi-stage amplifier design example provided illustrated how stability problems can exist within a design without being immediately obvious from top level simulations. In this example it was shown that by performing a thorough in-situ analysis of the amplifier the location of a stability problem was easily identified and located.

Possible future work includes developing more extensive stability analysis techniques that utilize some of the special properties of the in-situ analysis results. Such additions could include developing a means for renormalization of the in-situ transmission S-Parameters such that an accurate measure of in-situ gain or loss of a network component could be obtained. Another addition is to investigate the application of these techniques towards large signal simulations. This would allow the dynamic signal dependent behavior of network components to be obtained.

Appendix A

COUPLERS

A.1 Real

The following S-Matrix describes a typical loss-less passive coupler. The coupling factor is symmetric and is specified by C. The only contribution to the insertion loss of the through path is due to the energy lost to the coupled ports.

$$S_{coupler} = \begin{bmatrix} 0 & \sqrt{1-C^2} & C & 0 \\ \sqrt{1-C^2} & 0 & 0 & C \\ C & 0 & 0 & 0 \\ 0 & C & 0 & 0 \end{bmatrix} = \begin{bmatrix} S_{11} & S_{12} & S_{13} & S_{14} \\ S_{21} & S_{22} & S_{23} & S_{24} \\ S_{31} & S_{32} & S_{33} & S_{34} \\ S_{41} & S_{42} & S_{43} & S_{44} \end{bmatrix}$$

A.2 Ideal Unilateral Asymmetric Coupling

This is the coupler type used for all analysis in this document. This coupler is non-passive and provides a lossless zero-length through between the two through path ports of the coupler. The coupling from the trough path to the coupled ports is different than the coupling from the coupled ports into the through path. For the derivations provided above the value of $C_S$is set to unity, and the value for C_E is left as a variable C. The value for C can be set to unity as well if desired.

$$S_{coupler} = \begin{bmatrix} 0 & 1 & C_E & 0 \\ 1 & 0 & 0 & C_E \\ C_S & 0 & 0 & 0 \\ 0 & C_S & 0 & 0 \end{bmatrix}$$

Below is a Touchstone S-Parameter file that describes a coupler with the value of C set to 0.001. This S-Parameter file can be used to realize the necessary coupler behavior if an alternate means is not available in the simulation environment.

```
! ideal_coupler_60db.s4p
! Created by KMH
!
! Port 1 - Input Port
! Port 2 - Output Port
! Port 3 - Forward Port
! Port 4 - Reverse Port
!
! Provides 0dB path from P1 to P2
! Perfect isolation betwto P4
! -60 dB coupling from P3 to P1
! -60 dB coupling from P4 to P2
! Created Wed Jul 23 20:24:40 2008
! freq magS11 angS11 magS12 angS12 magS13 angS13 magS14 angS14
! magS21 angS21 magS22 angS22 magS23 angS23 magS24 angS24
! magS31 angS31 magS32 angS32 magS33 angS33 magS34 angS34
! magS41 angS41 magS42 angS42 magS43 angS43 magS44 angS44
!
# GHZ S MA R 50
0    0 0   1 0   1e-3 0   0 0
     1 0   0 0   0 0      1e-3 0
     1 0   0 0   0 0      0 0
     0 0   1 0   0 0      0 0
999  0 0   1 0   1e-3 0   0 0
     1 0   0 0   0 0      1e-3 0
     1 0   0 0   0 0      0 0
     0 0   1 0   0 0      0 0
```

REFERENCES

[1] K. Wang et al., "The S-probe a new, cost-effective, 4-Gamma method for evaluating mutli-stage amplifier stability" 1992 IEEE MTT-S Int.

[2] Microwave Symp. Dig., pp.829-832

[3] J. M. Rollett, “Stability and power gain invariants of linear two-ports," IRE Trans. Circuit Theory, Vol. 9, No. 3, 29-32, Mar. 1962.

[4] G. Gonzalez, Foundations of Oscillator Circuit Design. Norwood, MA: Artech House, 2007, ch 5, (5.6 pp. 276-280)

[5] Agilent Application Note 1462 ”Using Advanced Design System to Design an MMIC Amplifier”

[6] M.L. Edwards, J.H. Sinsky, “A new criterion for linear 2-port stability using a single geometrically derived parameter,“ IEEE Transactions on Microwave Theory and Techniques, Vol. 40, No. 12, 2303 - 2311, Dec. 1992

[7] R. Freitag, “A Unified Analysis of MMIC Power Amplifier Stability,” Microwave Symposium Digest, vol. 1, pp. 297-300, 1992.

[8] V. Gonzalez-Posadas, J. L. Jimenez-Martin, A. Parra- Cerrada1, D. Segovia-Vargas, and L. E. Garca-Munoz, “Oscillator Accurate Linear Analysis and Design. Classic Linear Methods Review and Comments,” Progress In Electromagnetics Research, vol. 118, pp. 89-116, 2011

[9] D., J. Esdale, M. J. Howes, “A reflection coeffcient approach to the design of one port negative impedance oscillators," IEEE Transactions on Mic. Theory and Techniques, Vol. 29, No. 8, 770-776, 1981.

[10] D. J. H. Maclean "Stability Margins in Microwave Amplifiers", IEEE Trans. on Microwave Theory and Techniques, vol. MTT-32, no. 3, pp.237 -242 1984

[11] Narhi, T.; Valtonen, M. "Stability envelope-new tool for generalised stability analysis", Microwave Symposium Digest, 1997., IEEE MTT-S International, On page(s): 623 - 626 vol.2 Volume: 2, 8-13 June 1997

[12] A. Platzker , W. Struble and K. Hetzler "Instability diagnosis and the role of K in microwave circuts", IEEE MTT-S Int. Microwave Symposium Digest, pp.1185 -1188 1993

[13] H. Patterson, "Signal Flow Graphs Simplify Microwave Circuit Analysis," Microwaves & RF, Aug., pp. 99-108 1995

[14] S.J. Mason, "Feedback Theory – Some Properties of Signal Flow Graphs," Proceedings of the IRE, Vol. 41, September 1953, pp. 1144-1156

[15] N. Kuhn, "Simplified Signal Flow Graph Analysis," Microwave Journal, Vol. 6, November 1963, pp. 59-66